

## Reassessing riverine carbon dioxide emissions from the Indian subcontinent

Omme K. Nayna<sup>a</sup>, Vedula V.S.S. Sarma<sup>b</sup>, Most Shirina Begum<sup>a</sup>, Jens Hartmann<sup>c</sup>, Sanjeev Kumar<sup>d</sup>, Shafi M. Tareq<sup>e</sup>, Ji-Hyung Park<sup>a</sup>

<sup>a</sup>Department of Environmental Science and Engineering, Ewha Womans University, Seoul 03760, Republic of Korea

<sup>b</sup>National Institute of Oceanography, Council of Scientific and Industrial Research, Visakhapatnam, India

<sup>c</sup>Institute for Geology, University of Hamburg, Hamburg 20146, Germany

<sup>d</sup>Geosciences Division, Physical Research Laboratory, Ahmedabad 380009, India

<sup>e</sup>Department of Environmental Sciences, Jahangirnagar University, Dhaka 1342, Bangladesh

Correspondence: Ji-Hyung Park, tel. +82-2-3277-2833, e-mail: jhp@ewha.ac.kr

### Abstract

While large rivers of the Indian subcontinent represent a “missing piece” of the global riverine CO<sub>2</sub> budget, anthropogenic perturbations are increasing uncertainties in estimating riverine CO<sub>2</sub> emissions via air-water CO<sub>2</sub> flux ( $F_{CO_2}$ ) from these rivers. This study aimed to provide an improved estimate of the total  $F_{CO_2}$  from the subcontinental rivers under increasing anthropogenic pressures by combining calculations of the partial pressure of CO<sub>2</sub> ( $pCO_2$ ) from water quality data of eight major rivers with new measurements in the Ganges and Godavari. The average  $pCO_2$  in the two newly surveyed rivers, including tributaries, wastewater drains, and impoundments, were 3–6 times greater than the previously reported values. In some urban tributaries and middle reaches of the Ganges that drain metropolitan areas, the measured  $pCO_2$  exceeded 20,000  $\mu\text{atm}$ , ~40 times the background level in the headwaters of the northern rivers. In the lower reaches of the Godavari,  $pCO_2$  reached 28,588  $\mu\text{atm}$ , seven times the mean  $pCO_2$  in the headwaters of the Deccan Traps. Across the northern rivers,  $pCO_2$  exhibited a significant negative relationship with dissolved oxygen, but a positive relationship with inorganic N or P concentrations. Thus, CO<sub>2</sub> emissions from hypoxic, eutrophic reaches can greatly exceed the phytoplanktonic CO<sub>2</sub> uptake. Spatially resolved  $pCO_2$  data, combined with three gas transfer velocity estimates, provided a higher range of  $F_{CO_2}$  from the subcontinental rivers (100.9–130.2 Tg CO<sub>2</sub>·yr<sup>-1</sup>) than the previous estimates (7.5–61.2 Tg CO<sub>2</sub>·yr<sup>-1</sup>). Given the revised estimates representing up to 5% of the global riverine  $F_{CO_2}$ , constraining the  $F_{CO_2}$  from the Indian subcontinental rivers would be a crucial step toward reducing the large uncertainty surrounding estimates of global inland waters  $F_{CO_2}$ .

**Keywords:** Carbon dioxide, Ganges River, Godavari River, Indian subcontinent, river impoundment, wastewater.

## 1. Introduction

Inland waters have been increasingly recognized as important sources of CO<sub>2</sub> and other greenhouse gases (GHGs) (Bastviken et al., 2011; Raymond et al., 2013; Lauerwald et al., 2015; Maavara et al., 2019). However, sparse field measurements in large river systems across Asia and Africa reveal many blind spots in the global riverine CO<sub>2</sub> emissions, contributing to large uncertainties in the global carbon budget (Raymond et al., 2013; Lauerwald et al., 2015; Park et al., 2018). Raymond et al. (2013) provided higher estimates of global riverine CO<sub>2</sub> emissions than Lauerwald et al. (2015), who did not consider CO<sub>2</sub> emissions from polluted rivers across Europe and America or streams with Strahler order <3. Although Asian rivers have been estimated to account for 40%–50% of the global inorganic and organic carbon fluxes from the land to the oceans (Degens et al., 1991; Ludwig et al., 1996; Schlunz and Schneider, 2000; Dai et al., 2012), large uncertainties remain regarding the contribution of increasingly polluted Asian rivers to global riverine CO<sub>2</sub> emissions (Li and Bush, 2015; Park et al., 2018). Spatially resolved field measurements of the partial pressure of CO<sub>2</sub> ( $p\text{CO}_2$ ) in large Asian rivers, particularly the monsoonal rivers across the Indian subcontinent (here we consider all or part of Bangladesh, Bhutan, India, Nepal, and Pakistan), have been suggested to reduce large uncertainties in estimating global riverine CO<sub>2</sub> emissions (Li and Bush, 2015; Park et al., 2018).

Anthropogenic perturbations, such as water pollution and impoundments, represent a primary source of uncertainty in global riverine C fluxes (Regnier et al., 2013). Wastewater can have severe environmental impacts on receiving rivers, particularly those downstream of rapidly expanding metropolitan areas (Yu et al., 2013; Yoon et al., 2017). Effluents from wastewater treatment plants (WWTPs) and agricultural runoffs loaded with organic matter and inorganic nutrients can alter the metabolic processes in the receiving river, often resulting in eutrophication, increases in the amount and lability of organic C, and emissions of CO<sub>2</sub> and other GHGs (Garnier et al., 2013; Burgos et al., 2015; Yoon et al., 2017). River impoundments can alter discharge and sediment transport (Syvitski et al., 2005) as well as riverine metabolic processes (Maavara et al., 2017). The altered metabolic processes in impounded rivers include increased rates of primary production and the subsequent reduction in CO<sub>2</sub> emissions (Liu et al., 2016; Jin et al., 2018). However, enhanced emissions have also been observed in the early years following dam construction (Abril et al., 2005; Shi et al., 2017) or from some impounded reaches and downstream estuaries under the influence of monsoon floods (Sarma et al., 2011; Prasad et al., 2013). Impoundment can also create longitudinal discontinuities in the transport of dissolved organic carbon (DOC) and nutrients across the impounded and downstream reaches, often accompanied by changes in  $p\text{CO}_2$  (Yoon et al., 2017; Jin et al., 2018).

River basins across the Indian subcontinent exhibit high levels of anthropogenic perturbations, including rapidly increasing water pollution and impoundments (Panneer Selvam et al., 2014; Li and Bush, 2015; Park et al., 2018). Urbanization and population growth in the Indian subcontinent have increased the annual production of municipal wastewater to  $19.3 \text{ km}^3 \cdot \text{yr}^{-1}$ , accounting for 6.2% of the global municipal wastewater production (Park et al., 2018). Despite reach-scale field studies on riverine  $\text{CO}_2$  emissions from large rivers such as the Ganges (Manaka et al., 2015; Dutta et al., 2019) and the Godavari (Prasad et al., 2013), only a few studies have been conducted to provide a regional-scale synthesis of riverine  $\text{CO}_2$  emissions from the Indian subcontinent (Panneer Selvam et al., 2014; Li and Bush, 2015). While Panneer Selvam et al. (2014) reported a relatively low estimate of  $\text{CO}_2$  emissions based on low-resolution measurements in 45 water bodies in Southern India, Li and Bush (2015) obtained higher estimates of riverine  $\text{CO}_2$  emissions from relatively high estimates of gas transfer velocity ( $k$ ). Moreover, neither of these previous estimates considered large variations in C fluxes between the monsoon and dry seasons, as found in the riverine organic matter fluxes (Ittekkot et al., 1985) and estuarine  $\text{CO}_2$  emissions (Dutta et al., 2019).

This study aimed to provide an improved regional estimate of  $\text{CO}_2$  emissions from the Indian subcontinental inland waters focusing on eight major rivers. We combined calculations of  $p\text{CO}_2$  from published water quality data and new field measurements in the Ganges and Godavari basins, used herein as the two representative systems under increasing anthropogenic pressures. Moreover, we assessed the anthropogenic impacts on riverine  $\text{CO}_2$  emissions by comparing  $p\text{CO}_2$  and other water quality variables among different river reaches and tributaries as well as between the monsoon and dry seasons. We expected that the estimate of riverine  $\text{CO}_2$  emissions from the Indian subcontinent would exceed the previous estimates if we take into consideration spatial and seasonal variations in  $p\text{CO}_2$  and river-specific gas transfer velocity ( $k$ ) estimates. To provide a reliable range of emissions estimates, not a single best estimate, we combined the spatially resolved data of  $p\text{CO}_2$  with three representative  $k$  values selected from the literature. We also tested whether the increasing discharge of untreated or poorly treated wastewater enhances  $\text{CO}_2$  emissions from eutrophic rivers draining large population centers, particularly during the dry periods.

## **2. Methods**

### **2.1. Study sites**

The study sites included the major branches and tributaries of the eight largest rivers of the Indian subcontinent (Fig. 1; Tables S1 and S2), which drain an area of  $\sim 3,504,000 \text{ km}^2$  (Milliman and Farnsworth, 2011). The basins share some common hydrological and demographic features,

including high population densities compared to the global average and a large seasonality in discharge (Table S1). These eight rivers were grouped into “the northern rivers” originating in the Himalayas (Ganges, Brahmaputra, and Indus) and “the Deccan Traps rivers” that either originate from the Deccan Traps (Narmada, Tapti, Godavari, and Krishna) or flow through an area connected to the Deccan Traps (Mahanadi). More details on the eight rivers are provided in supplementary information.

Literature data and recent field measurements were grouped into four categories: headwater streams, mainstems, tributaries, and impoundments (Fig. 1). Based on Strahler stream orders, the first-, second-, and third-order streams feeding into the upper end of mainstems and tributaries were considered as “headwaters” (Vannote et al., 1980; Lauerwald et al., 2015). The “mainstem” of each river was generally considered to begin at the confluence of more than two third-order headwater streams. Two major branches (Ganga and Yamuna) and two distributaries (Hooghly in India and Padma in Bangladesh) were considered to constitute the mainstems of the Ganges; the Indus and Sutlej branches as the Indus mainstems, Krishna and Bhima branches as the Krishna mainstems, and Tapti and Purna branches as the Tapti mainstems (Fig. 1). All other rivers consisted of a single mainstem. “Tributaries” are the first- or higher-order streams feeding into the aforementioned mainstems, excluding the uppermost reaches receiving headwaters. In the Ganges basin, wastewater drainages or polluted urban streams (“wastewater”) were additionally considered as local pollution sources that feed into the mainstem reaches within or downstream of the major metropolitan areas.

River impoundments, including dams, barrages, and weirs, are formed by constructing a barrier across the river to store water for power generation, irrigation, and domestic consumption (Space Applications Centre, 2011). In the Ganges mainstems, sampling was conducted at three impounded sites (Ganga Barrage, Dakpatthar Barrage, and Farakka Barrage), while literature data were used for six other impounded sites of the Indus mainstem (Jinnah Barrage, Chashma Barrage, Taunsa Barrage, Guddu Barrage, Sukkur Barrage, and Kotri Barrage). Ten impounded sites were sampled across the Godavari basin. Data were not available for any impoundment in the four other rivers of the Deccan Traps.

## **2.2. Field surveys in the Ganges and Godavari rivers**

To explore spatial and seasonal variations in riverine CO<sub>2</sub> concentrations and emissions across the Ganges (30°59'N, 78°56'E to 23°14'N, 90°38'E), samples were collected from August 2017 to February 2019 (Fig. 1; Table S2). These field surveys were conducted as part of a regional-scale study comparing the concentrations of three major GHGs (CO<sub>2</sub>, CH<sub>4</sub>, and N<sub>2</sub>O) in the Ganges,

Mekong, and Yellow rivers (Begum et al., 2021). CO<sub>2</sub> concentrations in the Ganges were used in this study to estimate riverine CO<sub>2</sub> emissions. Urban tributaries or wastewater drains were sampled together with the polluted reaches of the four main branches of the Ganges, within and downstream of the major metropolitan areas (Delhi, Kanpur, Varanasi, Kolkata, and Dhaka) (Fig. 1). Surface water *p*CO<sub>2</sub> was measured using a manual headspace equilibration method (Kling et al., 1992; Yoon et al., 2016). CO<sub>2</sub> concentrations in the equilibrated headspace air samples and the ambient air samples were measured on a gas chromatograph (7890A, Agilent, USA), which was equipped with a flame ionization detector coupled with a methanizer and a microelectron capture detector (Jin et al., 2018). Barometric pressure was measured using a portable sensor (Watchdog 1650 Micro Station, Spectrum Technologies Inc., USA). The CO<sub>2</sub> concentrations of the equilibrated and ambient air samples were used with barometric pressure and water temperature to calculate *p*CO<sub>2</sub> and CO<sub>2</sub> concentrations in the surface water based on Henry's law (Hudson, 2004).

Water samples were also collected from 10–20 cm below the water surface either directly in the bottle or via a portable water sampler (Masterflex E/S, Cole-Parmer, Illinois, USA) for chemical analysis. At the same time *in situ* water quality parameters including water temperature, pH, dissolved oxygen (DO), and electrical conductivity (EC) were measured using a portable multiparameter meter (Orion 5-Star Portable, Thermo Scientific, USA) at each sampling point. The samples were subsequently frozen and sent in an icebox to Korea within a week for chemical analysis in the laboratory. Water samples were filtered by pre-combusted (450°C) glass fiber filters (GF/F, Whatman; nominal pore size 0.7 μm) in the laboratory. Major inorganic ions including NO<sub>3</sub><sup>-</sup>, NH<sub>4</sub><sup>+</sup>, and PO<sub>4</sub><sup>3-</sup> dissolved in water were analyzed on an ion chromatograph (883 Basic IC Plus, Metrohm, Switzerland) and dissolved inorganic N (DIN) was calculated from total N concentration in NO<sub>3</sub><sup>-</sup> and NH<sub>4</sub><sup>+</sup>. For quality control of all the chemical analyses of the water samples, standards with known concentrations and ultrapure water were analyzed for each batch of ten samples, and triplicate analysis was performed for approximately 10% of all the samples to assess instrumental stability and accuracy. TA was analyzed with 40–80 mL filtered samples using an automated electric titrator (EasyPlus Titrator Easy pH, Metrohm, Switzerland) based on the Gran titration method. To determine the equivalence point at pH between 4 and 3, a strong acid (0.01 N HCl) was used to titrate (Gran, 1952).

Across the Godavari, two seasonal field surveys were conducted from headwater to mouth (20°00'N, 73°73'E to 17°02'N, 81°76'E) at 32 sites, including ten impounded locations, along the mainstem and tributaries during a monsoon (July-August) and a dry (March-April) period of 2012. Twenty-one sites along the upper, middle, and lower reaches of the mainstem and one site on an urban tributary

(Dharna River, 19°93'N, 73°86'E) were sampled during this period. Surface water samples were collected using 5 L Niskin bottles to analyze the pH and dissolved inorganic carbon (DIC). DIC was analyzed by coulometric titration using a coulometer (UIC Inc., USA). A portable conductivity-temperature-depth profiler (CTD; SBE-19 plus, Sea-Bird Electronics, USA) was used to measure water temperature and salinity.

### 2.3. Calculations of CO<sub>2</sub> concentrations and fluxes

#### 2.3.1. Calculation of pCO<sub>2</sub>

Water quality data, including pH, temperature, dissolved oxygen (DO), total alkalinity, NO<sub>3</sub><sup>-</sup>-N, and PO<sub>4</sub><sup>3-</sup>-P, were obtained from the Global River Chemistry database (GLORICH; Hartmann et al., 2014) and other published sources to calculate riverine pCO<sub>2</sub> and examine important environmental factors. The values of pCO<sub>2</sub> were calculated from alkalinity, pH, and water temperature using CO2SYS (Lewis and Wallace, 1998; Pierrot et al., 2006). In the case of the Hooghly and Godavari estuaries, we calculated pCO<sub>2</sub> from DIC, pH, water temperature, and salinity. To avoid potential overestimations of pCO<sub>2</sub> associated with organic acid contributions and increased sensitivity to alkalinity in acidic, organic-rich waters with low carbonate buffering capacity (Abril et al., 2015), we excluded all values of pCO<sub>2</sub> that were calculated from the input data with a pH < 5.5. Based on this criterion, we excluded pCO<sub>2</sub> values greater than 40,000 μatm at 9 sampling locations of the northern rivers among the total of 638 sampling locations of the subcontinental rivers.

#### 2.3.2. Calculation of air-water CO<sub>2</sub> flux

The air-water CO<sub>2</sub> flux ( $F_{CO_2}$ ) in a river system was calculated according to the equation (1).

$$F_{CO_2} = \Delta CO_2 \times k \times A_{river} \dots\dots\dots (1)$$

$\Delta CO_2$ ,  $k$ , and  $A_{river}$  represent the air-water CO<sub>2</sub> concentration gradient, the gas transfer velocity, and the river surface area, respectively (Wanninkhof et al., 2009; Raymond et al., 2012; Lauerwald et al., 2015).  $\Delta CO_2$  was calculated as the difference in pCO<sub>2</sub> between the surface water and ambient air, and then converted to the concentrations of CO<sub>2</sub> using the solubility coefficient of CO<sub>2</sub>,  $K_h$  (mmol m<sup>-3</sup> μatm<sup>-1</sup>) (Eq. 2). While the surface water pCO<sub>2</sub> was either measured or calculated as described in the preceding sections, an average atmospheric pCO<sub>2</sub> (436 μatm) was determined from our field measurements along the Ganges.  $K_h$  was calculated by using the equation (3) and the *in situ* water temperature ( $T_{water}$ ) estimated by the equation (4). The annual average air temperature at the sampling location,  $T_{air}$ , was used to estimate the annual average water temperature,  $T_{water}$  following Lauerwald et al. (2015).

$$\Delta CO_2 = K_h \times (pCO_{2\ water} - pCO_{2\ air}) \dots \dots \dots (2)$$

$$K_h = 10^{-(1.11+0.016 \times T - 0.00007 \times T^2)} \dots \dots \dots (3)$$

$$T_{water} [^\circ C] = 3.941 \pm 0.007 + 0.818 \pm 0.0004 T_{air} [^\circ C] \dots \dots \dots (4)$$

Annual average air temperatures were derived from an internet source (<https://www.timeanddate.com/weather/>). As input data required to calculate  $k$  using the widely used models (e.g., Raymond et al., 2012) were not available for many study sites of the eight rivers, we selected three published  $k$  values used for the similar streams and rivers in terms of the stream size and climate zone. The values of  $k_1$  and  $k_2$  were the minimum and the maximum of the  $k$  values used by Lauerwald et al. (2015) to calculate  $F_{CO_2}$  from the “streams and small rivers” or “large rivers” in the “temperate zone” (25°–50°) or “tropical zone” (<25°), respectively. Specific  $k_1$  and  $k_2$  values were selected based on the latitude of each site. Following the latitudinal zonation used by Lauerwald et al. (2015), the values of  $k_1$  (3.53–7.58 m day<sup>-1</sup>) and  $k_2$  (4.36–10.2 m day<sup>-1</sup>) calculated for the “streams and small rivers” were applied to the headwater stream and tributary sites, while those for “large rivers” were applied to the mainstem and impoundment sites. The values of  $k_3$  were taken as the averages of  $k$  values measured by Alin et al. (2011) in the large river reaches (width >100 m) and small tributaries and streams (width <100 m) of the Lower Mekong Basin. These two values of  $k_3$  were applied to the mainstem and impoundment sites (4.4 m day<sup>-1</sup>) or the headwater stream and tributary sites (6.7 m day<sup>-1</sup>).

To estimate the surface area of the subcontinental inland waters, we combined the published estimates for the surface areas of rivers, streams, reservoirs, and lakes. First, the surface area for the eight major river basins (21,251 km<sup>2</sup>) estimated at mean annual discharge was obtained from Allen and Pavelsky (2018). While the eight rivers account for 90% of the total discharge from the subcontinent (Milliman and Farnsworth, 2011), the surface area of the streams and rivers comprising the remaining 10% of discharge was estimated from the surface area of the eight rivers assuming a constant ratio for discharge to surface area. The surface areas for reservoirs and lakes in India were estimated for the pre-monsoon and post-monsoon season by Space Applications Centre (2011). The reservoirs and lakes in Bangladesh and Pakistan were excluded due to the lack of data. Therefore, combining the surface areas of the subcontinental rivers and India’s lakes and reservoirs yields a conservative estimate for the total surface area of the subcontinental inland waters.

The area-weighted mean areal  $F_{CO_2}$  (mmol m<sup>-2</sup> day<sup>-1</sup>) for each river basin was calculated from the mean areal  $F_{CO_2}$  and the surface area of each river component (headwaters, mainstems, tributaries, and impoundments). In the cases of the Ganges and Godavari, we calculated areal  $F_{CO_2}$  from the

mean  $p\text{CO}_2$  values of monsoon and dry-season measurements. For the rivers lacking data for one or more of the four river components, the mean areal  $F_{\text{CO}_2}$  was calculated from the values for the mainstems and tributaries (Tapti and Mahanadi) or the headwaters, mainstems, and tributaries (Brahmaputra, Narmada, and Krishna). The area-weighted mean areal  $F_{\text{CO}_2}$  for each river basin was multiplied by its total surface area to produce the total annual  $F_{\text{CO}_2}$ . The estimates of the annual  $F_{\text{CO}_2}$  were summed to obtain the total annual  $F_{\text{CO}_2}$  from the eight river basins.

To calculate uncertainty ranges of  $p\text{CO}_2$  and  $F_{\text{CO}_2}$  estimates, we used the Monte Carlo approach following Horgby et al. (2019). Based on the distribution of the  $p\text{CO}_2$  and  $F_{\text{CO}_2}$  values of each river basin, 10,000 sets of random data with 100 data points each were generated. The means of  $p\text{CO}_2$  and  $F_{\text{CO}_2}$  were calculated for each of these 10,000 sets of random data. Finally, the calculated 5th and 95th percentiles of the confidence interval for these means of  $p\text{CO}_2$  and  $F_{\text{CO}_2}$  were used to provide an uncertainty range. The calculated 5th and 95th percentiles of the confidence interval of  $F_{\text{CO}_2}$  were multiplied by the total surface area of the river basin to calculate the uncertainty range of the total annual  $F_{\text{CO}_2}$  for each river basin. The calculated uncertainty ranges of the total annual  $F_{\text{CO}_2}$  were summed to obtain the uncertainty range of the total annual  $F_{\text{CO}_2}$  from the eight rivers.

## 2.4. Statistical analyses

The relationships of  $p\text{CO}_2$  with other measured parameters, including temperature, pH, alkalinity, and DO, were analyzed by best-fit regressions in SigmaPlot (version 12). Regression analyses were also conducted to examine the relationship between inorganic nutrients ( $\text{NO}_3^-$ -N and  $\text{PO}_4^{3-}$ -P) and  $p\text{CO}_2$ . We conducted a t-test to explore the seasonal differences in  $p\text{CO}_2$  and  $F_{\text{CO}_2}$  for the mainstems, tributaries, and wastewater drains or urban streams in the Ganges basin. For this seasonal comparison, the headwater streams and impounded sites were included in the mainstem category. All statistical analyses were performed after applying the Shapiro-Wilk test to examine normal distribution of the data using SigmaPlot or R. Significance level was set at  $p < 0.05$ , unless mentioned otherwise.

## 3. Results

### 3.1. Variations in $p\text{CO}_2$ across the Indian subcontinent

The values of  $p\text{CO}_2$  calculated from water quality data, combined with measurements from the Ganges and Godavari, revealed large spatial variations in  $p\text{CO}_2$  among the headwaters, mainstems, tributaries, and impoundments across the eight river basins examined (Fig. 2; Table S3). In the three northern rivers,  $p\text{CO}_2$  was generally higher and more variable in the tributaries and mainstems than in the headwaters and impoundments. Meanwhile,  $p\text{CO}_2$  in the mainstems was similar to or even



higher than the levels found in the tributaries across the Deccan Traps. In the Godavari basin, the mainstems and impoundments exhibited the highest levels of  $p\text{CO}_2$ .

The average  $p\text{CO}_2$  measured in the Ganges and Godavari basins, including wastewater drains and impoundments, were respectively six and three times higher than those calculated from water quality data. The measured  $p\text{CO}_2$  reached up to 20,580  $\mu\text{atm}$  in the middle reach of the Yamuna traversing Delhi and 27,290  $\mu\text{atm}$  in a highly polluted urban tributary draining the Varanasi metropolitan area (Fig. 3c; Table S3). These values were over 40 times higher than the background levels found in the headwaters of the Ganges, Brahmaputra, and Indus (mean = 513; range: 150–1087  $\mu\text{atm}$ ; Figs. 2 and 3c). The spatial and seasonal variations in  $p\text{CO}_2$  across the Ganges basin revealed local hot spots corresponding to very high dry-season concentrations of biochemical oxygen demand (BOD) in highly polluted local urban tributaries and the downstream Yamuna reach (Fig. 4a; Central Pollution Control Board, 2014). Significantly higher values of  $p\text{CO}_2$  were observed in the tributaries during the dry season ( $p < 0.05$ ; Fig. 4a). The highest  $p\text{CO}_2$  in the Godavari (28,588  $\mu\text{atm}$ ) was seven times higher than the mean  $p\text{CO}_2$  found in the headwaters of the Deccan Traps (4,149  $\mu\text{atm}$ ) and that found at Rayapatnam Bridge near a fish market during the dry season (Figs. 2 and 3d; Table S3).

For the mainstem and tributary sites across the northern rivers (Ganges, Brahmaputra, and Indus), a significant positive relationship was observed between  $p\text{CO}_2$  and temperature ( $p < 0.0001$ ; Fig. 5a), in contrast to similarly strong negative relationships between  $p\text{CO}_2$ , pH, and DO ( $p < 0.001$ ; Figs. 5c and d). A significant positive relationship was also observed between  $p\text{CO}_2$  and total alkalinity in the mainstems and tributaries across the northern rivers ( $p < 0.0001$ ; Fig. 5b). Compared to the mainstems of the northern rivers, larger deviations from the regressions were caused by extremely high levels of  $p\text{CO}_2$  in several polluted tributaries and wastewater drains. A significant negative relationship was observed between  $p\text{CO}_2$  and pH in the mainstems and tributaries across the Deccan Traps ( $p < 0.001$ ; Fig. S1). When the pH- $p\text{CO}_2$  relationship of the mainstems was compared with the tributaries across the Deccan Traps rivers, larger deviations from the regressions were caused by extremely high levels of  $p\text{CO}_2$  in several polluted mainstem reaches. Similarly, when the pH- $p\text{CO}_2$  relationship of the tributaries was compared between the northern and Deccan Traps rivers, larger deviations were found in some mainstems and tributaries of the northern rivers. A significant positive relationship was found between  $p\text{CO}_2$  and air temperature across the subcontinental rivers ( $p < 0.01$ ; Fig. S4).

Across the subcontinental rivers, the levels of  $p\text{CO}_2$ , dissolved inorganic nitrogen ( $\text{DIN} = \text{NO}_3^- + \text{NH}_4^+$ ), and  $\text{PO}_4^{3-}\text{-P}$  were generally higher and more variable in the tributaries than in the mainstems and headwaters (Fig. S2). The concentrations of  $\text{NO}_3^-$ -DIN in the impounded sites across the Ganges, Indus, and Godavari basins were lower than those in the mainstems and tributaries. Compared to the

Godavari basin, relatively high concentrations of  $\text{PO}_4^{3-}\text{-P}$  were found in the impounded reaches of the Indus basin (Fig. S2A). Across the northern rivers, a significant positive relationship was observed between  $p\text{CO}_2$  and  $\text{NO}_3^-\text{-N}$  only in the tributaries ( $p < 0.001$ ; Fig. 6a), whereas  $p\text{CO}_2$  and  $\text{PO}_4^{3-}\text{-P}$  were positively correlated in both the mainstems and tributaries ( $p < 0.001$ ; Fig. 6b). In contrast, the rivers in the Deccan Traps exhibited a significant negative relationship between  $p\text{CO}_2$  and  $\text{NO}_3^-\text{-N}$  in the tributaries ( $p < 0.05$ ; Fig. 6c). A limited number of  $\text{PO}_4^{3-}\text{-P}$  data available for the Godavari river exhibited no significant relationship with  $p\text{CO}_2$  (Fig. 6d).

### 3.2. Regional estimates for riverine $\text{CO}_2$ emissions

The  $F_{\text{CO}_2}$  per unit surface area displayed large spatial variations across the subcontinent, ranging from  $-9.3$  to  $355.7 \text{ g CO}_2 \cdot \text{m}^{-2} \cdot \text{d}^{-1}$  (Table S4). The values of  $F_{\text{CO}_2}$  estimated for the mainstems of the northern rivers tended to be lower than those of the Deccan Traps rivers (Table S4). Across the northern rivers, the estimated  $F_{\text{CO}_2}$  was generally higher in the tributaries and mainstems compared to the headwaters and impounded reaches, reflecting the contribution of  $F_{\text{CO}_2}$  from polluted urban tributaries and downstream river sections, respectively (Table S4). A relatively low range of  $F_{\text{CO}_2}$  from  $-4.7$  to  $10.7 \text{ g CO}_2 \cdot \text{m}^{-2} \cdot \text{d}^{-1}$  was estimated for the headwater streams of the northern rivers, while generally larger values were estimated for the headwater streams of the Deccan Traps ( $7.1$ – $159.2 \text{ g CO}_2 \cdot \text{m}^{-2} \cdot \text{d}^{-1}$ ; Table S4). The  $F_{\text{CO}_2}$  estimates for the impounded reaches of the Ganges and Indus averaged  $1.7 \text{ g CO}_2 \cdot \text{m}^{-2} \cdot \text{d}^{-1}$ , which was much lower than that of the impounded reaches in the Godavari basin ( $85.4 \text{ g CO}_2 \cdot \text{m}^{-2} \cdot \text{yr}^{-1}$ ; Table S4).

The estimated surface area of  $21,251 \text{ km}^2$  for the eight major rivers consisted of  $17,595 \text{ km}^2$  for the northern rivers and  $3,656 \text{ km}^2$  for the Deccan Traps rivers, accounting for  $\sim 3\%$  of the global streams and rivers ( $773,000 \text{ km}^2$ ; Allen and Pavelsky, 2018). Among the northern and Deccan Traps rivers, the Ganges and Godavari accounted for the largest shares of  $A_{\text{river}}$  and  $F_{\text{CO}_2}$ , respectively (Table 1). The high  $F_{\text{CO}_2}$  values, combined with the large  $A_{\text{river}}$ , produced high annual total  $F_{\text{CO}_2}$  estimates for the Ganges and Godavari (Table 1). In these basins, new measurements of  $p\text{CO}_2$  from the headwater streams through several polluted urban tributaries to the lowest reaches (Table S3) contributed to the relatively high  $F_{\text{CO}_2}$  values.

The annual  $F_{\text{CO}_2}$  from the eight rivers averaged  $100.9 \text{ Tg CO}_2 \cdot \text{yr}^{-1}$ , with an uncertainty range of  $97.6$  to  $104.2 \text{ Tg CO}_2 \cdot \text{yr}^{-1}$  (Table 1). The annual  $F_{\text{CO}_2}$  estimated for the entire subcontinental rivers ( $23,376 \text{ km}^2$ ) averaged  $110.9 \text{ Tg CO}_2 \cdot \text{yr}^{-1}$ , with an uncertainty range of  $107.3$  to  $114.6 \text{ Tg CO}_2 \cdot \text{yr}^{-1}$  (Table 1). The surface area of the lakes ( $3,262 \text{ km}^2$ ) and reservoirs ( $17,644 \text{ km}^2$ ) in India estimated

by Space Applications Centre (2011) was added to the estimated river surface area to obtain a conservative estimate of the total area for the subcontinental inland waters (44,282 km<sup>2</sup>). The estimates of the combined inland waters  $F_{CO_2}$  varied from 102.7 to 132.0 Tg CO<sub>2</sub> yr<sup>-1</sup> depending on the selected value of  $k$ , averaging 112.7 Tg CO<sub>2</sub> yr<sup>-1</sup> with an uncertainty range of 109.1 to 116.4 Tg CO<sub>2</sub>·yr<sup>-1</sup> (Fig. 7).

## 4. Discussion

### 4.1. Regional patterns of riverine $pCO_2$

The combination of literature data and new measurements revealed some distinct spatial patterns, as illustrated by the higher levels of  $pCO_2$  in the urban tributaries and receiving mainstem reaches than the background levels found in the headwater streams of the northern rivers (Fig. 2; Table S3). This longitudinal pattern of downriver increases in  $pCO_2$  is contradictory to recent global syntheses that have found higher  $pCO_2$  in low-order streams due to the release of CO<sub>2</sub> derived from soil respiration and the dilution of soil-derived CO<sub>2</sub> in larger streams and rivers with increasing stream order (Lauerwald et al., 2015; Marx et al., 2017). The relatively low  $pCO_2$  values (mean: 513  $\mu$ atm) found in the headwater streams of the northern rivers compared to those found in the Deccan Traps rivers (mean: 4,149  $\mu$ atm) can be attributed to active carbonate weathering in the carbonate-rich terrain of the Himalayas (Dalai et al., 2002; Chakrapani and Veizer, 2005). In contrast, the relatively high  $pCO_2$  values in the headwater streams of the Deccan Traps rivers may be partly associated with the silicate weathering in the Deccan volcanic terrain rich in granite and basalt, which creates favorable conditions for physical and chemical weathering at high temperature and runoff (Dessert et al., 2001; Das et al., 2005). An unusually high  $pCO_2$  (12,177  $\mu$ atm) in a headwater stream of the Godavari basin may reflect enhanced decomposition of forest detritus and organic pollutants derived from agricultural runoff during the dry season (Balakrishna and Probst, 2005).

In the Ganges, the input of poorly treated wastewater to the middle and lower reaches may contribute to large increases in  $pCO_2$  in the urban tributaries and receiving rivers along large metropolitan and industrial areas (Park et al., 2018), as compared to the relatively low levels of  $pCO_2$  in the headwater streams draining carbonate-rich mountainous areas of the Himalayas (Dalai et al., 2002; Chakrapani and Veizer, 2005). The higher dry-season  $pCO_2$  in the tributaries and mainstem reaches of the Ganges (Fig. 4a) suggest that wastewater-derived, labile organic matter (OM) might be more susceptible to photo- and biodegradation under the conditions of increased light intensities and reduced flows (Prasad et al., 2013; Wang et al., 2017a; Yoon et al., 2017). The dry-season increases in  $pCO_2$  are contrary to the previous reports on monsoonal floods transferring loads of CO<sub>2</sub> and

labile OM from terrestrial sources (Ittekkot et al., 1985; Li et al., 2013; Jin et al., 2018). The extremely high levels of  $p\text{CO}_2$  observed in the Yamuna are consistent with significantly higher levels of BOD in the waters draining the metropolitan areas of Delhi and Agra. This indicates that localized peaks of  $p\text{CO}_2$  may be directly associated with BOD loadings or indirectly with the wastewater-boosted biodegradation of riverine organic matter (Begum et al., 2019, 2021). The BOD concentrations measured in the Ganges during 1986–2014 exhibited a longitudinal pattern that peaked in the Yamuna reaches near Delhi and decreased along the river (Central Pollution Control Board, 2014), consistent with a model-based prediction (Wen et al., 2017).

In the Deccan Traps, the highest levels of  $p\text{CO}_2$  were found in the mainstem reaches of the Godavari during the dry season, implying large sources of labile OM, including forest detritus, municipal wastewater, and agricultural runoff from the expanding urban and agricultural activities in the heavily forested basin (Sarin et al., 2002; Sarma et al., 2011; Prasad et al., 2013). Particularly high levels of  $p\text{CO}_2$  (7541–28,588  $\mu\text{atm}$ ) found in the middle and lower reaches of the Godavari traversing the urban areas may result from enhanced biodegradation of terrestrial OM by wastewater-derived labile OM under the conditions of reduced flows during dry periods (Chavan et al., 2010; United Nations Environmental Program, 2016). Compared with the  $p\text{CO}_2$  values reported in the present study, literature-derived  $p\text{CO}_2$  estimates were relatively low across the Godavari basin (Figs. 3b, d). Relatively low levels of  $p\text{CO}_2$  in the impounded reaches of the northern rivers (Fig. 2) indicated an enhanced phytoplanktonic  $\text{CO}_2$  uptake, which has been suggested by the inverse relationship between primary production and  $p\text{CO}_2$  observed in the impounded reaches of the Mississippi (Crawford et al., 2016), Yangtze (Liu et al., 2016), Yellow River (Ran et al., 2017), and Han River (Jin et al., 2018). River impoundments increase water residence time and sedimentation but decrease turbidity, creating favorable conditions for the phytoplanktonic uptake of  $\text{CO}_2$  (Deemer et al., 2016; Prairie et al., 2018). However, the unusually high levels of  $p\text{CO}_2$  found in the impounded reaches of the Godavari basin during the dry season suggest that large inputs of wastewater into the impounded waters that remain stagnant for several months due to dam closures can facilitate the bacterial decomposition of labile OM, thus elevating the level of  $p\text{CO}_2$  (Prasad et al., 2013). High  $\text{CO}_2$  emissions from the impounded reaches and downstream estuaries of the Godavari during the monsoon season have been attributed to the enhanced decomposition of the allochthonous OM in the eutrophic impounded reaches exceeding the phytoplanktonic uptake of  $\text{CO}_2$  (Ittekkot et al., 1985; Sarma et al., 2011; Prasad et al., 2013).

Significant relationships between  $p\text{CO}_2$  and other water quality parameters in the mainstems, tributaries, and impoundments in the subcontinental rivers (Figs. 5, S1) can help decipher the role of

water pollution in the large spatiotemporal variations of  $p\text{CO}_2$ . The relationships between water quality and  $p\text{CO}_2$  reflected general characteristics found in polluted urban river systems, including high alkalinity and lowered pH and DO (Kaushal et al., 2014; Smith et al., 2017; Wang et al., 2017b; Li et al., 2020). Significant negative relationships between  $p\text{CO}_2$  and pH for the mainstems and tributaries (Figs. 5c, S1) suggest that discharge of acid anions such as sulfates and/or acidic DOM components could decrease pH, thus increasing  $p\text{CO}_2$  and creating hotspots of riverine  $\text{CO}_2$  emissions as observed in other urban rivers (Chen et al., 2002; Wang et al., 2017b, Jin et al., 2018). The significant positive relationship between  $p\text{CO}_2$  and water temperature in the mainstems and tributaries of the northern rivers (Fig. 5a), along with the similar relationship between  $p\text{CO}_2$  and air temperature found for all subcontinental rivers (Fig. S4), may reflect either a large input of  $\text{CO}_2$  from terrestrial sources or an enhanced degradation of OM fueling riverine  $F_{\text{CO}_2}$  *in situ* during the warmer monsoon season (Borges et al., 2018; Jin et al., 2018). The significant negative relationship between DO and  $p\text{CO}_2$  for the mainstems, tributaries, and impoundments in the northern rivers (Fig. 5d) suggest that enhanced respiration in the water column and anaerobic sediment could lead to low DO and high  $p\text{CO}_2$ , consistent with previous research on urban rivers (Noriega and Araujo, 2014; Wang et al., 2017b; Jin et al., 2018). This result conforms to the hypothesis that urbanization intensifies the transformation of rivers from autotrophic to heterotrophic systems (Smith and Kaushal, 2015).

Elevated DIN concentrations in the tributaries compared to the mainstems and headwaters in the two sub-regions (Fig. S2) underline the role of anthropogenic nutrients from large population centers in urbanized river reaches (Kaushal et al., 2014). High loadings of  $\text{NO}_3^-$  and  $\text{PO}_4^{3-}$  can alter the riverine metabolic processes involved in  $\text{CO}_2$  uptake and release in very complex ways (Wang et al., 2017b; Li et al., 2020). For example, phytoplankton blooms can enhance  $\text{CO}_2$  uptake in the early phase, while labile organic materials released from phytoplankton biomass can also fuel bacterial decomposition of the bulk OM pool, resulting in increased  $\text{CO}_2$  production (Cole and Caraco, 2001; Begum et al., 2019). Therefore, the significant positive relationships between  $p\text{CO}_2$  and  $\text{NO}_3^-$ -N or  $\text{PO}_4^{3-}$ -P observed for the mainstems and tributaries in the northern rivers (Fig. 6a, b) suggest that accelerated OM degradation in the eutrophic, anoxic reaches may enhance  $\text{CO}_2$  emissions to the degree exceeding the phytoplanktonic  $\text{CO}_2$  uptake (Wang et al., 2017b; Li et al., 2020). In contrast, the significant negative relationship between  $p\text{CO}_2$  and  $\text{NO}_3^-$ -N found for the tributaries in the Deccan Traps rivers (Fig. 6c) implies that algal photosynthesis may still act as a primary sink of  $\text{CO}_2$  at the current eutrophic level (Wang et al., 2017b; Jin et al., 2018). These seemingly contrasting relationships are consistent with the prediction that increasing nutrient loadings in urbanized rivers

may alter the balance between photosynthesis and respiration to a tipping point beyond which the river shifts to a heterotrophic system (Wang et al., 2017b; Yoon et al., 2017).

#### 4.2. Constraining estimates of riverine CO<sub>2</sub> emissions from the Indian subcontinent

Previous regional and global estimates of riverine CO<sub>2</sub> emissions did not fully consider the differences in emission rates among headwater streams, mainstems, tributaries, and impoundments, nor between the seasons with distinct differences in discharge. Accounting for these differences allowed our approach to provide more resolved data of  $F_{CO_2}$  for the classified river components. The average  $F_{CO_2}$  per unit surface area for the mainstems of the Deccan Traps rivers (39.2 g CO<sub>2</sub>·m<sup>-2</sup>·d<sup>-1</sup>; Table S4) was higher than the global average (15.8 g CO<sub>2</sub>·m<sup>-2</sup>·d<sup>-1</sup>) reported by Lauerwald et al. (2015), while the average  $F_{CO_2}$  estimated for the mainstems of the northern rivers (3.5 g CO<sub>2</sub>·m<sup>-2</sup>·d<sup>-1</sup>; Table S4) was lower than the global average. The regional difference in geology between the carbonate-dominated northern rivers and the Deccan Traps of volcanic origin can partly explain the large differences in  $pCO_2$  levels observed in the headwater streams (Table S3). The high  $F_{CO_2}$  values observed in the Deccan Traps rivers may also result from enhanced decomposition of allochthonous OM derived from plants and anthropogenic sources. Given the fact that no direct  $pCO_2$  has been measured in these rivers, the accuracy of  $F_{CO_2}$  estimation needs to be improved by direct measurements of  $pCO_2$ .

Despite the relatively low levels of  $pCO_2$  and  $F_{CO_2}$  in the northern rivers compared to those for the Deccan Traps rivers, our measured  $pCO_2$  values in the Ganges basin resulted in higher estimates of  $F_{CO_2}$  per unit surface area than the estimates based on calculated  $pCO_2$  from published water quality data (Fig. S3a). These results might be due to an inaccuracy in calculating  $pCO_2$  from water quality data collected by previous studies over a long span of years. For instance, such a small difference as 0.1 in pH unit can result in a 20% change in the calculated value of  $pCO_2$  (Lauerwald et al., 2013). Alternatively, our approach took into consideration the highly polluted urban tributaries, wastewater drains, and impacted mainstem reaches, as well as seasonality (Figs. S3a and 4b). Localized increases in  $F_{CO_2}$  from polluted urban tributaries, mainstems, and impounded reaches emphasize the importance of incorporating anthropogenically impacted rivers in the regional and global riverine carbon budget. As these localized increases in  $F_{CO_2}$  were combined with the large surface area ( $A_{river}$ ), the total annual  $F_{CO_2}$  estimated for the Ganges was highest among the subcontinental rivers (Table 1).

While many dams and barrages have been constructed on the mainstems and tributaries of the subcontinental rivers, there are still substantial uncertainties surrounding  $F_{CO_2}$  from the impounded reaches across the region due to the scarcity of monitoring data (Park et al., 2018) and the variability in the observed impoundment effects in the northern rivers and Godavari (Table S3; Sarma et al., 2011; Prasad et al., 2013). These uncertainties have been reflected in the wide range of reported  $F_{CO_2}$  estimates from reservoirs and barrages in the Indian subcontinent. For instance, Li and Bush (2015) reported a relatively high estimate (3.08 Tg CO<sub>2</sub>·yr<sup>-1</sup>) for the impounded reaches of large Indian rivers without the use of direct measurements of  $pCO_2$ , whereas Panneer Selvam et al. (2014) provided a more conservative  $F_{CO_2}$  estimate for all of the reservoirs in India, based on their measurements in South India (2.37 Tg CO<sub>2</sub>·yr<sup>-1</sup>).

Scaling-up the previously reported mean areal  $F_{CO_2}$ , including 20 mmol m<sup>-2</sup> day<sup>-1</sup> (Panneer Selvam et al., 2014) and 163 mmol m<sup>-2</sup> day<sup>-1</sup> (Li and Bush, 2015), to the estimated surface area of the subcontinental rivers (23,376 km<sup>2</sup>; Table 1) produces 7.5 and 61.2 Tg CO<sub>2</sub>·yr<sup>-1</sup>, respectively. Our estimates of the annual  $F_{CO_2}$  for the subcontinental rivers (100.9–130.2 Tg CO<sub>2</sub>·yr<sup>-1</sup>; Table 1) are higher than the estimates based on Panneer Selvam et al. (2014) and Li and Bush (2015) by a factor of up to 17. Similarly, scaling up the previously reported average areal  $F_{CO_2}$  from lakes and reservoirs (5.3 mmol·m<sup>-2</sup>·day<sup>-1</sup>; Panneer Selvam et al., 2014) to the total estimated surface area in India (20,906 km<sup>2</sup>; Space Applications Centre, 2011) resulted in an estimate of 1.8 Tg CO<sub>2</sub>·yr<sup>-1</sup>. The lakes and reservoirs outside of India were not considered herein, so we may have obtained a conservative estimate of inland waters  $F_{CO_2}$  from the subcontinent, which averaged 112.7 Tg CO<sub>2</sub> yr<sup>-1</sup>, spanning 102.7–132.0 Tg CO<sub>2</sub> yr<sup>-1</sup> (Fig. 7). The combined inland waters  $F_{CO_2}$  of the Indian subcontinent based on previously reported values was estimated at 9.3 and 63.0 Tg CO<sub>2</sub> yr<sup>-1</sup>, respectively (Fig. 7; Panneer Selvam et al., 2014; Li and Bush, 2015).

Panneer Selvam et al. (2014) provided the first national-scale quantification of CO<sub>2</sub> emissions from the inland waters of India based on field measurements of  $pCO_2$  in South India, but they could not fully address data scarcity for large river systems. Moreover, they did not include data from reservoirs that were later recognized as significant sources of CO<sub>2</sub> emissions (Li and Bush, 2015). A follow-up study by Li and Bush (2015) provided higher  $F_{CO_2}$  estimates by incorporating literature  $pCO_2$  data and relatively high  $k$  values based on wind speed following a study conducted in the Mekong River (Alin et al., 2011). Although Li and Bush (2015) used literature-based  $pCO_2$  data for seven major rivers of India, their data could not adequately cover the lower reaches of the mainstems and seasonal differences between the dry and monsoon seasons. Moreover, their study did not

consider the polluted urban tributaries and impounded reaches, which have been identified as significant sources of CO<sub>2</sub> emissions by this study and other studies (Paner Selvam et al., 2014; Park et al., 2018; Begum et al., 2021). Our estimates of the combined inland waters  $F_{CO_2}$  of 102.7 to 132.0 Tg CO<sub>2</sub> yr<sup>-1</sup> exceed the estimates based on Paner Selvam et al. (2014) and Li and Bush (2015) by a factor of up to 14 (Fig. 7). Our estimates included more spatially resolved data from headwater streams to lower reaches of the rivers, except Tapti and Krishna. Moreover, we included two seasonal datasets for most of the rivers, except Krishna and Tapti. Our study considered the effects of increasing anthropogenic impacts by adding data from polluted urban tributaries or wastewater drains and affected mainstem reaches of the Ganges and impounded reaches of the three large river basins (Indus, Ganges, and Godavari).

In the regional-scale carbon budgets of South Asia, riverine carbon transport, net ecosystem productivity, and land-use change were considered significant carbon sinks (147 Tg C·yr<sup>-1</sup>; Patra et al., 2013), and riverine CO<sub>2</sub> emissions were not considered due to the lack of data. The estimated CO<sub>2</sub> emissions from the subcontinental inland waters (mean: 31 Tg C·yr<sup>-1</sup>, with an uncertainty range of 30 to 32 Tg C·yr<sup>-1</sup> from Monte Carlo simulations) comprise 21% (20–22%) of the estimated total terrestrial carbon sink of South Asia. The estimates of the subcontinental riverine  $F_{CO_2}$  account for 2–5% of the global riverine  $F_{CO_2}$  (Table 1). This is consistent with the global spatial patterns of  $F_{CO_2}$  identified by Lauerwald et al. (2015), which illustrated that the Ganges and large rivers in China between 25°N and 30°N represent the second peak in latitudinal gradient, next to the tropical rivers between 10°N and 10°S. Thus, the estimated rates of inland water CO<sub>2</sub> emissions are high enough to change the continental to global budgets of CO<sub>2</sub>. It can therefore be assumed that the current subcontinental C fluxes are likely to be considerably underestimated.

### 4.3. Uncertainty analysis

Limited availability of input data for the three main components of the  $F_{CO_2}$  equation demands special care in comparing the estimated regional riverine CO<sub>2</sub> emission with previous estimates. First, the spatial extent of streams and rivers, including accounted stream orders and surface area, can exert a strong influence on the potential range of  $F_{CO_2}$ . To estimate the global river surface area, Downing et al. (2012) first established stream-order scaling relationships between the width and length of the river under the assumption that all rivers belong to a single branching river network. They provided two estimates of the global river surface area, including 485,000 km<sup>2</sup> for rivers wider than 90 m and 682,000 km<sup>2</sup> based on the length and width of the Amazon River. Raymond et al. (2013) applied flow routing algorithm to digital topography to get the total estimate of 536,000 km<sup>2</sup> excluding



Greenland, Antarctica, and seasonal effects of freezing rivers. Both studies are constrained by the lack of direct measurements of surface area, the quantification of statistical uncertainties, and consideration of regional variability in hydraulic geometry. Allen and Pavelsky (2018) used satellite images and a statistical method to produce a more direct estimation of the global river surface area. Their estimate of 773,000 km<sup>2</sup> at annual average discharge, excluding reservoirs, lakes, canals, Antarctica, Greenland, and any water bodies measured at mean sea level, is 44% higher than the estimates provided by Raymond et al. (2013).

Lauerwald et al. (2015) accounted for 10 stream orders in their synthesis of global riverine CO<sub>2</sub> emissions, excluding the first- and second-order streams that comprise about 10% of the estimated global river surface area but can make a disproportionate contribution to the global  $F_{CO_2}$  due to the generally high ranges of  $pCO_2$  and  $k$  observed across different climate zones (Marx et al., 2017). Allen and Pavelsky (2018) included the headwater streams in their estimates of the surface area of each river basin. We calculated the surface area of the headwater streams (Strahler stream order 1 to 3; Downing et al., 2012) based on the reported fraction of the total surface area of headwater streams in the global river surface area (17.4%, Marx et al., 2017). The total surface area of headwater streams estimated for the subcontinental rivers (4,067 km<sup>2</sup>) can make a disproportionate contribution to the regional  $F_{CO_2}$  due to the relatively low or high ranges of  $pCO_2$  observed in the northern rivers and the Deccan Traps rivers, respectively.

More accurate estimates of  $k$  in streams and rivers under various flow conditions are another prerequisite to constrain  $F_{CO_2}$  estimates from the subcontinental rivers. Our regional estimates of riverine  $F_{CO_2}$  were based on the carefully selected three  $k$  values. The values of  $k_1$  and  $k_2$  were derived from two empirical equations with different datasets of flow and weather conditions (Lauerwald et al., 2015). Stream flow velocity, width, and depth are the major controlling factors of  $k$  for small streams and rivers (Raymond et al., 2012), whereas in larger rivers  $k$  may be also controlled by wind effects (Alin et al., 2011). The empirical equations employed by Lauerwald et al. (2015) are based solely on a few of these controlling factors, ignoring the potentially large influence of others. Further efforts are required to improve  $k$  estimates, such as field measurements of site-specific river discharge and wind speed.

We calculated  $pCO_2$  from water temperature, pH, and alkalinity, each of which might be subject to considerable uncertainties (Butman and Raymond, 2011; Raymond et al., 2013; Lauerwald et al., 2015). The difference in pH of 0.1 units can lead to a change in the calculated values of  $pCO_2$  by 20% (Lauerwald et al., 2013). Across the Indian subcontinent, we calculated monthly values of  $pCO_2$ , and

the average value of  $p\text{CO}_2$  was taken for a single site if seasonal measurements were available. We discarded samples with pH lower than 5.5 because the calculations of  $p\text{CO}_2$  from such low pH values are too uncertain, mainly because of noncarbonate contribution in the alkalinity (Hunt et al., 2011). Field measurements of  $p\text{CO}_2$  are necessary to reduce the uncertainty associated with  $p\text{CO}_2$  calculation.

Given the downriver increases in  $p\text{CO}_2$  along the large metropolitan and industrial areas of the Ganges basin, our estimates of  $p\text{CO}_2$  and  $F_{\text{CO}_2}$  per unit surface area might be conservative, above all due to the lack of tributary and lower-reach data in the Krishna and Tapti. It would also be essential to perform samplings across the monsoon and dry seasons for all rivers in the subcontinent in order to account for large seasonal differences in riverine  $F_{\text{CO}_2}$ . Although both monsoon and dry seasons were covered in the Ganges, Indus, Narmada, and Godavari basins, more monsoonal data than dry-season data were accounted for the other rivers. Additional field measurements in important hot spots, such as urban tributaries and wastewater drains, also need to be obtained across the seasons to reflect the effect of increasing pollution on the riverine  $F_{\text{CO}_2}$  from the Indian subcontinent (Begum et al., 2021).

## 5. Conclusions

The spatially resolved  $p\text{CO}_2$  data integrating literature data and new field measurements in the Ganges and Godavari, combined with three wide-ranging  $k$  estimates, provided significantly higher estimates of  $F_{\text{CO}_2}$  from the Indian subcontinental rivers than the previous estimates. The large differences between these estimates illustrate the substantial uncertainty associated with  $k$  and other factors required for calculating  $F_{\text{CO}_2}$ . Neglecting localized  $F_{\text{CO}_2}$  peaks from highly polluted tributaries and impacted river reaches can cause further uncertainty. Field surveys in the Ganges and Godavari basins revealed large inputs of  $\text{CO}_2$  and labile organic matter via poorly treated wastewater from metropolitan areas, which would provide increasingly important sources for the  $F_{\text{CO}_2}$  from eutrophic, and often hypoxic, downriver reaches. The exceptionally high levels of  $p\text{CO}_2$  in the urban tributaries and downriver reaches of the Ganges contributed significantly to the revised estimate of  $F_{\text{CO}_2}$  from the basin. These localized pollution patterns are currently not captured by conservative  $F_{\text{CO}_2}$  estimates for other understudied rivers across the region. The overall results suggest that providing spatially resolved data of  $p\text{CO}_2$  and  $k$ , together with considering the localized pollution effects on urban tributaries and receiving rivers that greatly vary with seasonal changes in discharge, can better constrain the estimates of  $F_{\text{CO}_2}$  from understudied river systems not only in the subcontinent but also worldwide. The results also illustrate the importance of considering inland water  $\text{CO}_2$  emissions from

the subcontinent to reduce the large uncertainty associated with the continental and global carbon budgets. Further research is required to elucidate the role of nutrient and oxygen availability in enhancing heterotrophy in urbanized rivers and concomitant riverine CO<sub>2</sub> emissions.

### **Acknowledgements**

This work was supported by the Asia-Pacific Network for Global Change Research (CRRP2016-01MY-Park) and the National Research Foundation of Korea funded by the Korean Government (NRF-2017R1D1A1B06035179).

### **Data availability**

Data are available and can be requested from the corresponding author (jhp@ewha.ac.kr).

### **Author contribution**

The study was designed by OKN and JHP. OKN performed all data works with additional inputs from JHP, JH, SK, SMT, and MSB; while JHP, OKN, and MSB, and VVSSS conducted field surveys in the Ganges and Godavari, respectively. The manuscript was written by OKN and JHP, with contributions from all coauthors.

### **Competing interests**

The authors declare that they have no conflict of interest.

### **References**

- Abril, G., Guérin, F., Richard, S., Delmas, R., Galy-Lacaux, C., Gosse, P., Tremblay, A., Varfalvy, L., Dos Santos, M. A., Matvienko, B., 2005. Carbon dioxide and methane emissions and the carbon budget of a 10-year old tropical reservoir (Petit Saut, French Guiana). *Global Biogeochem. Cycles* 19, <https://doi.org/10.1029/2005GB002457>
- Abril, G., Bouillon, S., Darchambeau, F., Teodoru, C. R., Marwick, T. R., Tamooh, F., Ochiengo Omengo, F., Geeraert, N., Deirmendjian, L., Polsenaere, P., Borges, A. V., 2015. Technical Note: large overestimation of  $p\text{CO}_2$  calculated from pH and alkalinity in acidic, organic-rich freshwaters. *Biogeosciences* 12, 67–78. <https://doi.org/10.5194/bg-12-67-2015>
- Allen, G. H., Pavelsky, T. M., 2018. Global extent of rivers and streams. *Science* 361, 585–588. <https://doi.org/10.1126/science.aat0636>
- Alin, S. R., Rasera, M. F. F. L., Salimon, C. I., Richey, J. E., Holtgrieve, G. W., Krusche, A. V., Snidvongs, A., 2011. Physical controls on carbon dioxide transfer velocity and flux in low-gradient river systems and implications for regional carbon budgets. *J. Geophys. Res.* 116, <https://doi.org/10.1029/2010JG001398>
- Balakrishna, K., Probst, J. L., 2005. Organic carbon transport and C/N ratio variations in a large tropical river: Godavari as a case study, India. *Biogeochemistry* 73, 457–473. <https://doi.org/10.1007/s10533-004-0879-2>

- Bastviken, D., Tranvik L. J., Downing, J. A., Crill, P. M., Enrich-Prast, A. 2011. Freshwater methane emissions offset the continental carbon sink. *Science* 331, <https://doi.org/10.1126/science.1196808>
- Begum, M. S., Jang, I., Lee, J.-M., Oh, H. B., Jin, H., Park, J.-H., 2019. Synergistic effects of urban tributary mixing on dissolved organic matter biodegradation in an impounded river system. *Sci. Total Environ.* 676, 105–119. <https://doi.org/10.1016/j.scitotenv.2019.04.123>
- Begum, M. S., Bogard, M., Butman, D., Chea, E., Kumar, S., Lu, X. X., Nayna, O. K., Ran, L., Richey, J. E., Tareq, S. M., Verma, S., Thi Xuan, D., Yu, R., Park, J.-H., 2021. Localized pollution impacts on CO<sub>2</sub>, CH<sub>4</sub>, and N<sub>2</sub>O dynamics in three anthropogenically modified Asian river systems. *J. Geophys. Res. Biogeosci.* 126, <https://doi.org/10.1029/2020JG006124>
- Borges, A. V., Drachambeau, F., Teodoru, C.R., Marwick, T. R., Tamooh, F., Geeraert, N., 2015. Globally significant greenhouse-gas emissions from African inland waters. *Nat. Geosci.* 8, 637–642. <https://doi.org/10.1038/ngeo2486>
- Borges, A. V., Darchambeau, F., Lambert, T., Bouillon, S., Morana, C., Brouyere, S., Hakoun, V., Jurado, A., Tseng, H.C., Descy, J.-P., Roland, F. A. E., 2018. Effects of agricultural land use on fluvial carbon dioxide, methane and nitrous oxide concentrations in a large European river, the Meuse (Belgium). *Sci. Total Environ.* 610–611, 342–355. <https://doi.org/10.1016/j.scitotenv.2017.08.047>
- Butman, D., Raymond, P. A., 2011. Significant efflux of carbon dioxide from streams and rivers in the United States. *Nat. Geosci.* 4, 839–842. <https://doi.org/10.1038/ngeo1294>
- Central Pollution Control Board, 2014. India. <https://cpcb.nic.in/nwmp-data-2014/> (accessed 31 December 2020)
- Chakrapani, G. J., Veizer, J., 2005. Dissolved inorganic carbon isotopic compositions in the upstream Ganga River in the Himalayas. *Curr. Sci.* 89, 553–556.
- Chavan, A. D., Sharma, M. P., Bargava, R., 2010. Water quality assessment of the Godavari River. *Hydro Nepal J. Water Energy Environ.* 5, 31–34. <https://doi.org/10.3126/hn.v5i0.2483>
- Chen, J., Wang, F., Xia, X., Zhang, L., 2002. Major element chemistry of the Changjiang (Yangtze River). *Chem. Geol.* 187, 231–255, [https://doi.org/10.1016/s0009-2541\(02\)00032-3](https://doi.org/10.1016/s0009-2541(02)00032-3)
- Cole, J. J., Caraco, N. F., 2001. Carbon in catchments: Connecting terrestrial carbon losses with aquatic metabolism. *Mar. Freshw. Res.* 52, 101–110. <https://doi.org/10.1071/MF00084>
- Crawford, J. T., Loken, L. C., Stanley, E. H., Stets, E. G., Dornblaser, M. M., Striegl, R. G., 2016. Basin scale controls on CO<sub>2</sub> and CH<sub>4</sub> emissions from the Upper Mississippi River. *Geophys. Res. Lett.* 43, 1973–1979. <https://doi.org/10.1002/2015GL067599>
- Dai, M., Yin, Z., Meng, F., Liu, Q., Cai, W.J., 2012. Spatial distribution of riverine DOC inputs to the ocean: an updated global synthesis. *Curr. Opin. Environ. Sustain.* 4, 170–178. <https://doi.org/10.1016/j.cosust.2012.03.003>
- Dalai, T. K., Krishnaswami, S., Sarin, M. M., 2002. Major ion chemistry in the headwaters of the Yamuna river system: chemical weathering, its temperature dependence and CO<sub>2</sub> consumptions

in the Himalaya. *Geochim. Cosmochim. Acta* 66, 3397–3416. [https://doi.org/ 10.1016/S0016-7037\(02\)00937-7](https://doi.org/10.1016/S0016-7037(02)00937-7)

- Das, A., Krishnaswami, S., Sarin, M. M., Pande, K., 2005. Chemical weathering in the Krishna basin and Western Ghats of the Deccan Traps, India: rates of basalt weathering and their controls. *Geochim. Cosmochim. Acta* 69, 2067–2084. [https://doi.org/ 10.1016/j.gca.2004.10.014](https://doi.org/10.1016/j.gca.2004.10.014)
- Degens, E. T., Kempe, S., Richey, J. E., 1991. *Biogeochemistry of major world rivers*. Chichester: Published on behalf of the Scientific Committee on Problems of the Environment (SCOPE) of the International Council of Scientific Unions (ICSU), and the United Nations Environment Programme (UNEP) by Wiley.
- Deemer, B. R., Harrison, J. A., Li, S., Beaulieu, J. J., Delsontro, T., Barros, N., Bezerra-Neto, J. F., Powers, S. M., dos Santos, M. A., Vonk, J. A., 2016. Greenhouse gas emissions from reservoir water surfaces: a new global synthesis. *BioScience*, 66, 949–964. <https://doi.org/10.1093/biosci/biw117>
- Dessert, C., Dupre, B., Francois, L. M., Schott, J., Gaillardet, J., Chakrapani, G., Bajpai, S., 2001. Erosion of Deccan Traps determined by river geochemistry: impact on the global climate and the  $^{87}\text{Sr}/^{86}\text{Sr}$  ratio of seawater. *Earth Planet. Sci. Lett.* 188, 459–474. [https://doi.org/10.1016/S0012-821X\(01\)00317-X](https://doi.org/10.1016/S0012-821X(01)00317-X)
- Downing, J. A., Cole, J. J., Duarte, C. M., Middelburg, J. J., Melack, J. M., Prairie, Y. T., Kortelainen, P., Striegl, R. G., McDowell, W. H., Tranvik, L. J., 2012. Global abundance and size distribution of streams and rivers. *Inland Waters* 2, 229–236. <https://doi.org/10.5268/IW-2.4.502>
- Dutta, M. K., Kumar, S., Mukherjee, R., Sanyal, P., Mukhopadhyay, S. K., 2019. The post-monsoon carbon biogeochemistry of the Hooghly-Sundarbans estuarine system under different levels of anthropogenic impacts. *Biogeosciences*, 16, 289–307. <https://doi.org/10.5194/bg-16-289-2019>
- Garnier, J., Vilain, G., Silvestre, M., Billen, G., Jehanno, S., Poirier, D., Martinez, A., Decuq, C., Cellier, P., Abril, G., 2013. Budget of methane emissions from soils, livestock and the river network at the regional scale of the Seine basin (France). *Biogeochemistry* 116, 199–214. <https://doi.org/10.1007/s10533-013-9845-1>
- Gupta, H., Chakrapani, G. J., Selvaraj, K., Kao, S. J., 2011. The fluvial geochemistry, contributions of silicate, carbonate, and saline–alkaline components to chemical weathering flux and controlling parameters: Narmada River (Deccan Traps), India. *Geochim. Cosmochim. Acta* 75, 800–824. <https://doi.org/10.1016/j.gca.2010.11.010>
- Hartmann, J., Lauerwald, R., Moosdorf, N., 2014. A brief overview of the GLObal River Chemistry Database, GLORICH. *Procedia Earth. Planet. Sci.* 10, 23–27. <https://doi.org/10.1016/j.proeps.2014.08.005>
- Hudson, F., 2004. Sample preparation and calculations for dissolved gas analysis in water samples using GC headspace equilibration technique. RSKSOP-175, Revision No. 2, U.S. Environmental Protection Agency, USA.
- Hunt, C. W., Salisbury, J. E., Vandemark, D., 2011. Contribution of non-carbonate anions to total alkalinity and overestimation of  $p\text{CO}_2$  in New England and New Brunswick rivers. *Biogeosciences*, 8, 3069–3076. <https://doi.org/10.5194/bg-8-3069-2011>

- Ittekkot, V., Safiullah, S., Mycke, B., Seifert, R., 1985. Seasonal variability and geochemical significance of organic matter in the River Ganges, Bangladesh. *Nature*, 317, 800–802. <https://doi.org/10.1038/317800a0>
- Jin, H., Yoon, T. K., Begum, M. S., Lee, E.-J., Oh, N.-H., Kang, N., Park, J.-H., 2018. Longitudinal discontinuities in riverine greenhouse gas dynamics generated by dams and urban wastewater. *Biogeosciences*, 15, 6349–6369. <https://doi.org/10.5194/bg-2018-278>
- Kaushal, S. S., Mayer, P. M., Vidon, P. G., Smith, R. M., Pennino, M. J., Duan, S. W., Newcomer, T. A., Welty, C., Belt, K. T., 2014. Land use and climate variability amplify carbon, nutrient, and contaminant pulses: a review with management implications. *J. Am. Water Res. Assoc.* 50, 585–614. <https://doi.org/10.1111/jawr.12204>
- Kling, G., Kipphut, G., Miller, M., 1992. The flux of CO<sub>2</sub> and CH<sub>4</sub> from lakes and rivers in arctic Alaska. *Hydrobiologia* 240, 23–36. <https://doi.org/10.1007/BF00013449>
- Lauerwald, R., J. Hartmann, N. Moosdorf, S. Kempe, Raymond, P. A., 2013. What controls the spatial patterns of the riverine carbonate system? a case study for North America. *Chem. Geol.* 337–338, 114–127. <https://doi.org/10.1016/j.chemgeo.2012.11.011>.
- Lauerwald, R., Laruelle, G. G., Hartmann, J., Ciais, P., Regnier, P. A. G., 2015. Spatial patterns in CO<sub>2</sub> evasion from the global river network. *Global Biogeochem. Cycles* 29, 534–554. <https://doi.org/10.1002/2014GB004941>
- Lewis, E., Wallace, D., 1998. Program developed for CO<sub>2</sub> system calculations. United States. <https://doi.org/10.2172/639712>.
- Li, S. Y., Lu, X. X., Bush, R. T., 2013. CO<sub>2</sub> partial pressure and CO<sub>2</sub> emission in the Lower Mekong River. *J. Hydrol.* 504, 40–56. <https://doi.org/10.1016/j.jhydrol.2013.09.024>
- Li, S., Bush, R. T., 2015. Revision of methane and carbon dioxide emissions from inland waters in India. *Glob. Change Biol.* 21, 6–8. <https://doi.org/10.1111/gcb.12705>
- Li, S., Luo, J., Wu, D., Xu, Y. J., 2020. Carbon and nutrients as indicators of daily fluctuations of pCO<sub>2</sub> and CO<sub>2</sub> flux in a river draining a rapidly urbanizing area. *Ecol. Indic.* 109, <https://doi.org/10.1016/j.ecolind.2019.105821>
- Liu, S., Lu, X. X., Xia, X., Zhang, S., Ran, L., Yang, X., Liu, T., 2016. Dynamic biogeochemical controls on river pCO<sub>2</sub> and recent changes under aggravating river impoundment: an example of the subtropical Yangtze River. *Global Biogeochem. Cycles* 30, 880–897, <https://doi.org/10.1002/2016GB005388>
- Ludwig, W., Probst, J.-L., Kempe, S., 1996. Predicting the oceanic input of organic carbon by continental erosion. *Global Biogeochem. Cycles* 10, 23–41. <https://doi.org/10.1029/95GB02925>
- Maavara, T., Lauerwald, R., Regnier, P., Van Cappellen, P., 2017. Global perturbation of organic carbon cycling by river damming. *Nat. Commun.* 8, <https://doi.org/10.1038/ncomms15347>
- Maavara, T., Lauerwald, R., Laruelle, G. G., Akbarzadeh, Z., Bouskill, N. J., Cappellen, P. V., Regnier, P., 2019. Nitrous oxide emissions from inland waters: are IPCC estimates too high? *Glob. Change Biol.* 25, 473–488. <https://doi.org/10.1111/gcb.14504>

- Manaka, T., Ushie, H., Araoka, D., Otani, S., Inamura, A., Suzuki, A., Zakir Hossain, H. M., Kawahata, H., 2015. Spatial and seasonal variation in surface water  $p\text{CO}_2$  in the Ganges, Brahmaputra, and Meghna Rivers on the Indian Subcontinent. *Aquat. Geochem.* 21, 437–458. <https://doi.org/10.1007/s10498-015-9262-2>
- Marx, A., Dusek, J., Jankovec, J., Sanda, M., Vogel, T., Van Geldern, R., Hartmann, J., Barth, J. A. C., 2017. A review of  $\text{CO}_2$  and associated carbon dynamics in headwater streams: a global perspective. *Rev. Geophys.* 55, 560–585. <https://doi.org/10.1002/2016RG000547>
- Milliman, J. D., Farnsworth, K. L., 2011. River discharge to the coastal ocean: a global synthesis. Cambridge University Press, Cambridge, UK, 13–69.
- Millero, F. J., 1979. The thermodynamics of the carbonic acid system in seawater. *Geochim. Cosmochim. Acta* 43, 1651–1661. [https://doi.org/10.1016/0016-7037\(79\)90184-4](https://doi.org/10.1016/0016-7037(79)90184-4)
- Noriega, C., Araujo, M., 2014. Carbon dioxide emissions from estuaries of north and northeastern Brazil. *Sci. Rep.* 4, <https://doi.org/10.1038/srep06164>
- Panneer Selvam, B., Natchimuthu, S., Arunachalam, L., Bastviken, D., 2014. Methane and carbon dioxide emissions from inland waters in India - implications for large scale greenhouse gas balances. *Glob. Change Biol.* 20, 3397–3407. <https://doi.org/10.1111/gcb.1257520>
- Park, J.-H., Nayna, O. K., Begum, M. S., Chea, E., Hartmann, J., Keil, R. G., Kumar, S., Lu, X., Ran, L., Richey, J.E., Sarma, V.V.S.S., Tareq, S.M., Thi Xuan, D., Yu, R., 2018. Reviews and syntheses: anthropogenic perturbations to carbon fluxes in Asian river systems – concepts, emerging trends, and research challenges. *Biogeosciences* 15, 3049–3069. <https://doi.org/10.5194/bg-2017-549>
- Patra, P. K., Canadell, J. G., Houghton, R. A., Piao, S. L., Oh, N.-H., Ciais, P., Manjunath, K. R., Chhabra, A., Wang, T., Bhattacharya, T., Bousquet, P., Hartman, J., Ito, A., Mayorga, E., Niwa, Y., Raymond, P. A., Sarma, V. V. S. S., Lasco, R., 2013. The carbon budgets of South Asia. *Biogeosciences* 10, 513–527. <https://doi.org/10.5194/bg-10-513-2013>
- Pierrot, D., Lewis, E., Wallace, D. W. R., 2006. MS Excel program developed for  $\text{CO}_2$  system calculations, ORNL/CDIAC-105a, Carbon dioxide Information Analysis Center, Oak Ridge National Laboratory, U.S. Department of Energy, Oak Ridge, Tennessee (Vol. 3).
- Prairie, Y. T., Alm, J., Beaulieu, J., Barros, N., Battin, T., Cole, J., Giorgio, P., DelSontro, T., Guérin, F., Harby, A., Harrison, J., Mercier-Blais, S., Serça, D., Sobek, S., Vachon, D., 2018. Greenhouse gas emissions from freshwater reservoirs: what does the atmosphere see? *Ecosystems* 21, 1058–1071. <https://doi.org/10.1007/s10021-017-0198-9>
- Prasad, M. H. K., Sarma, V. V. S. S., Krishna, M. S., Reddy, N. P. C., 2013. Carbon dioxide emissions from the tropical Dowleiswaram reservoir on the Godavari River, Southeast of India. *J. Water Resour. Prot.* 5, 534–545. <https://doi.org/10.4236/jwarp>
- Ran, L., Li, L., Tian, M., Yang, X., Yu, R., Zhao, J., Wang, L., Lu, X. X., 2017. Riverine  $\text{CO}_2$  emissions in the Wuding River catchment on the Loess Plateau: environmental controls and dam impoundment impact. *J. Geophys. Res. Biogeosci.* 122, 1439–1455. <https://doi.org/10.1002/2016JG003713>

- Raymond, P. A., Zappa, C. J., Butman, D., Bott, T. L., Potter, J., Mulholland, P., Laursen, A. E., McDowell, W. H., Newbold, D., 2012. Scaling the gas transfer velocity and hydraulic geometry in streams and small rivers. *Limnol. Oceanogr. Fluids Environ.* 2, 41–53. <https://doi.org/10.1215/21573689-1597669>
- Raymond, P. A., Hartmann, J., Lauerwald, R., Sobek, S., McDonald, C., Hoover, M., Butman, D., Striegl, R., Mayorga, E., Humborg, C., Kortelainen, P., Durr, H., Meybeck, M., Ciais, P., Guth, P., 2013. Global carbon dioxide emissions from inland waters. *Nature*, 503, 355–359. <https://doi.org/10.1038/nature12760>
- Regnier, P., Friedlingstein, P., Ciais, P., Mackenzie, F. T., Gruber, N., Janssens, I. A., Laruelle, G. G., Lauerwald, R., Luyssaert, S., Andersson, A. J., Arndt, S., Arnosti, C., Borges, A. V., Dale, A. W., Gallego-Sala, A., Godd ris, Y., Goossens, N., Hartmann, J., Heinze, C., Ilyina, T., Joos, F., Larowe, D. E., Leifeld, J., Meysman, F. J. R., Munhoven, G., Raymond, P. A., Spahni, R., Suntharalingam, P., Thullner, M., 2013. Anthropogenic perturbation of the carbon fluxes from land to ocean. *Nat. Geosci.* 6, 597–607. <https://doi.org/10.1038/ngeo1830>
- Space Applications Centre, 2011. National Wetland Atlas, India. SAC/EPISA/ABHG/NWIA/ATLAS/34/2011.
- Sarin, M. M., Sudheer, A. K., Balakrishna, K., 2002. Significance of riverine carbon transport: a case study of a large tropical river, Godavari (India). *Sci. China Ser. C Life Sci.* 45, 97–108.
- Sarma, V. V. S. S., Kumar, N. A., Prasad, V. R., Venkataramana, V., Appalanaidu, S., Sridevi, B., Kumar, B. S. K., Bharati, M. D., Subbaiah, C. V., Acharyya, T., Rao, G. D., Viswanadham, R., Gawade, L., Manjary, D. T., Kumar, P. P., Rajeev, K., Reddy, N. P. C., Sarma, V. V., Kumar, M. D., Sadhuram, Y., Murty, T. V. R., 2011. High CO<sub>2</sub> emissions from the tropical Godavari estuary (India) associated with monsoon river discharges. *Geophys. Res. Lett.* 38, <https://doi.org/10.1029/2011GL046928>
- Schl nz, B., Schneider, R. R., 2000. Transport of terrestrial organic carbon to the oceans by rivers: re-estimating flux- and burial rates. *Int. J. Earth Sci.* 88, 599–606. <https://doi.org/10.1007/s005310050>
- Shi, W., Chen, Q., Yi, Q., Yu, J., Ji, Y., Hu, L., Chen, Y., 2017. Carbon emission from cascade reservoirs: spatial heterogeneity and mechanisms. *Environ. Sci. Technol.* 51, 12175–12181. <https://doi.org/10.1021/acs.est.7b03590>
- Smith, R. M., Kaushal, S. S., Beaulieu, J. J., Pennino, M. J., Welty, C., 2017. Influence of infrastructure on water quality and greenhouse gas dynamics in urban streams. *Biogeosciences*, 14, 2831–2849. <https://doi.org/10.5194/bg-14-2831-2017>
- Smith, R. M., Kaushal, S. S., 2015. Carbon cycle of an urban watershed: exports, sources, and metabolism. *Biogeochemistry* 126, 173–195. <https://doi.org/10.1007/s10533-015-0151-y>
- Syvitski, J. P. M., V r smarty, C. J., Kettner, A. J., Green, P., 2005. Impact of humans on the flux of terrestrial sediment to the global coastal ocean. *Science* 308, 376–380. <https://doi.org/10.1126/science.1109454>



- United Nations Environmental Program, 2016. A snapshot of the world's water quality: towards a global assessment. [https://uneplive.unep.org/media/docs/assessments/unep\\_wwqa\\_report\\_web.pdf](https://uneplive.unep.org/media/docs/assessments/unep_wwqa_report_web.pdf)
- Vannote, R. L., Minshall, G. W., Cummins, K. W., Sedell, J. R., Cushing, C. E., 1980. The river continuum concept. *Can. J. Fish. Aquat. Sci.* 37, 130–137. <https://doi.org/10.1139/f80-017>
- Wang, X., He, Y., Yuan, X., Chen, H., Peng, C., Yue, J., Zhang, Q., Diao, Y., Liu, S., 2017a. Greenhouse gases concentrations and fluxes from subtropical small reservoirs in relation with watershed urbanization. *Atmos. Environ.* 154, 225–235. <https://doi.org/10.1016/j.atmosenv.2017.01.047>
- Wang, X. F., He, Y. X., Yuan, X. Z., Chen, H., Peng, C. H., Zhu, Q., Yue, J., Ren, H., Deng, W., Liu, H. 2017b.  $p\text{CO}_2$  and  $\text{CO}_2$  fluxes of the metropolitan river network in relation to the urbanization of Chongqing, China. *J. Geophys. Res. Biogeosci.* 122, 470–486. <https://doi.org/10.1002/2016G003494>
- Wen, Y., Schoups, G., van de Giesen, N., 2017. Organic pollution of rivers: Combined threats of urbanization, livestock farming and global climate change. *Sci. Rep.* 7, <https://doi.org/10.1038/srep43289>
- Weiss, R. F., 1974. Carbon dioxide in water and seawater: the solubility of a non-ideal gas. *Mar. Chem.* 2, 203–215. [https://doi.org/10.1016/0304-4203\(74\)90015-2](https://doi.org/10.1016/0304-4203(74)90015-2)
- Wanninkhof, R., Asher, W. E., Ho, D. T., Sweeney, C., McGillis, W. R., 2009. Advances in quantifying air-sea gas exchange and environmental forcing. *Annu. Rev. Mar. Science*, 1, 213–244. <https://doi.org/10.1146/annurev.marine.010908.163742>
- Yoon, T. K., Jin, H., Oh, N.-H., Park, J.-H., 2016. Technical note: assessing gas equilibration systems for continuous  $p\text{CO}_2$  measurements in inland waters. *Biogeosciences* 13, 3915–3930. <https://doi.org/10.5194/bg-13-3915-2016>
- Yoon, T. K., Jin, H., Begum, M. S., Kang, N., Park, J.-H., 2017.  $\text{CO}_2$  outgassing from an urbanized river system fueled by wastewater treatment plant effluents. *Environ. Sci. Technol.* 51, 10459–10467. <https://doi.org/10.1021/acs.est.7b02344>
- Yu, G.-R., Zhu, X.-J., Fu, Y.-L., He, H.-L., Wang, Q.-F., Wen, X.-F., Li, X.-R., Zhang, L.-M., Zhang, L., Su, W., Li, S.-G., Sun, X.-M., Zhang, J.-H., Yan, J.-H., Wang, H.-M., Zhou, G.-S., Jia, B.-R., Xiang, W.-H., Li, Y.-N., Zhao, L., Wang, Y.-F., Shi, P.-L., Chen, S.-P., Xin, X.-P., Zhao, F.-H., Wang, Y.-Y., Tong, C.-L., 2013. Spatial patterns and climate drivers of carbon fluxes in terrestrial ecosystems of China. *Glob. Change Biol.* 19, 798–810. <https://doi.org/10.1111/gcb.12079>

Table 1: Summary of  $p\text{CO}_2$  and the mean areal and annual  $\text{CO}_2$  emissions ( $F_{\text{CO}_2}$ ) estimated for the eight major rivers and all rivers of the Indian subcontinent. The 5th and 95th percentiles of confidence interval from Monte Carlo simulations are provided in parentheses as uncertainty ranges. Refer to Methods for the three gas transfer velocity ( $k$ ) values selected to estimate  $\text{CO}_2$  emissions.

Rivers	Area $\text{km}^2$ $\times 10^3$	$p\text{CO}_2$ ( $\mu\text{atm}$ )	Mean areal $F_{\text{CO}_2}$ ( $\text{g CO}_2 \cdot \text{m}^{-2} \cdot \text{d}^{-1}$ )			Annual $F_{\text{CO}_2}$ ( $\text{Tg CO}_2 \cdot \text{yr}^{-1}$ )		
			$k1$	$k2$	$k3$	$k1$	$k2$	$k3$
Indus	3.61	725	2.7	3.6	2.5	3.6	4.7	3.3
		(717–734)	(2.6–2.8)	(3.5–3.8)	(2.4–2.6)	(3.4–3.7)	(4.6–5.0)	(3.2–3.4)
Ganges	8.06	1538	10.2	13.2	10.1	30.0	38.9	29.7
		(1511–1571)	(9.6–10.7)	(12.4–14.0)	(9.5–10.6)	(28.3–31.5)	(36.5–41.2)	(28.0–31.2)
Brahmaputra	5.92	1059	9.4	12.6	8.3	20.3	27.2	17.9
		(1034–1085)	(9.1–9.8)	(12.2–13.1)	(8.0–8.6)	(19.7–21.2)	(26.4–28.3)	(17.3–18.6)
Narmada	0.46	3377	21.3	26.9	23.3	3.61	4.6	3.94
		(3343–3415)	(21.0–21.5)	(26.6–27.3)	(22.9–23.6)	(3.55–3.64)	(4.5–4.62)	(3.88–3.99)
Tapti	0.22	1886	12.5	16.1	12.9	1.02	1.31	1.05
		(1873–1899)	(12.3–12.6)	(16.0–16.3)	(12.8–13.0)	(1.00–1.03)	(1.3–1.33)	(1.04–1.06)
Mahanadi	0.70	2036	12.1	16.0	13.2	3.10	4.1	3.38
		(2026–2045)	(12.0–12.2)	(15.9–16.1)	(13.1–13.3)	(3.07–3.12)	(4.0–4.12)	(3.35–3.40)
Godavari	1.25	9599	54.8	68.0	61.0	25.0	31.1	27.9
		(9507–9705)	(54.2–55.4)	(67.2–68.7)	(60.2–61.7)	(24.8–25.3)	(30.7–31.4)	(27.5–28.2)
Krishna	1.02	2045	13.7	17.6	14.1	5.1	6.53	5.23

		(2025–2068)	(13.5–13.9)	(17.4–17.9)	(14.0–14.4)	(5.0–5.2)	(6.46–6.64)	(5.20–5.35)
8 Rivers	21.2 <sup>a</sup>	2783	17.1	21.8	18.2	91.7	118.4	92.4
		(2755–2815)	(16.8–17.4)	(21.4–22.2)	(17.9–18.5)	(88.8–94.6)	(114.5–122.6)	(89.4–95.2)
Indian subcontinent	23.3 <sup>b</sup>					100.9	130.2	101.7
						(97.6–104.1)	(126.0–134.9)	(98.3–104.7)
World	536	3100				6600 <sup>c</sup>		
		(0–100 000)						
World	699–832	2400 (2019–2826)	15.8 (12.4–19.5)			2383 <sup>d</sup>		

<sup>a</sup>Surface area of 8 large rivers of the subcontinent; <sup>b</sup>Surface area of all rivers and streams of the subcontinent; <sup>c</sup>Total annual  $F_{CO_2}$  for the global rivers and streams (Raymond et al., 2013); <sup>d</sup>Total annual  $F_{CO_2}$  for the global rivers and streams (Lauerwald et al., 2015); Three gas transfer velocity ( $k$ ) values ( $k_1$ – $k_3$ ) used for  $F_{CO_2}$  estimates in the subcontinental rivers, provide the ranges of  $k$  value, including, for Deccan Traps rivers (Narmada, Tapti, Mahanadi, Godavari, and Krishna),  $k_1$ : 3.53–6.90  $m \cdot d^{-1}$ ,  $k_2$ : 4.36–8.86  $m \cdot d^{-1}$ , and  $k_3$ : 4.4–6.7  $m \cdot d^{-1}$ ; for northern rivers (Indus, Ganges, and Brahmaputra),  $k_1$ : 3.53–7.58  $m \cdot d^{-1}$ ,  $k_2$ : 4.36–10.2  $m \cdot d^{-1}$ , and  $k_3$ : 4.4–6.7  $m \cdot d^{-1}$ .

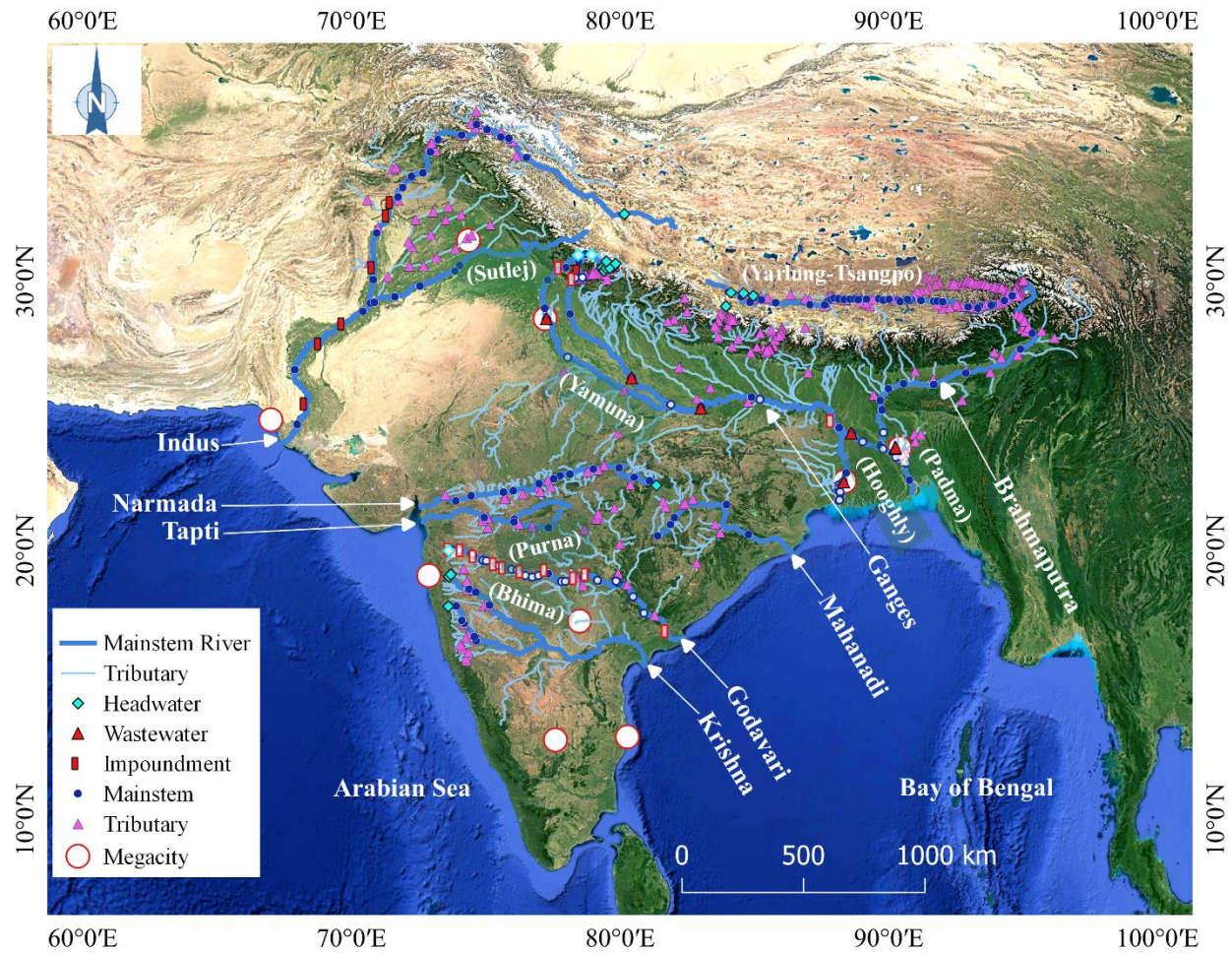


Fig. 1. Study map showing the sampling sites along the headwater, mainstem, impoundment, tributary, and wastewater across the eight major river basins of the Indian subcontinent. Our own field measurement sites on the Ganges and Godavari are indicated by void symbols, while sites for literature data are indicated by filled symbols. Major branches of eight rivers that constitute mainstems are indicated by putting their names in parentheses.

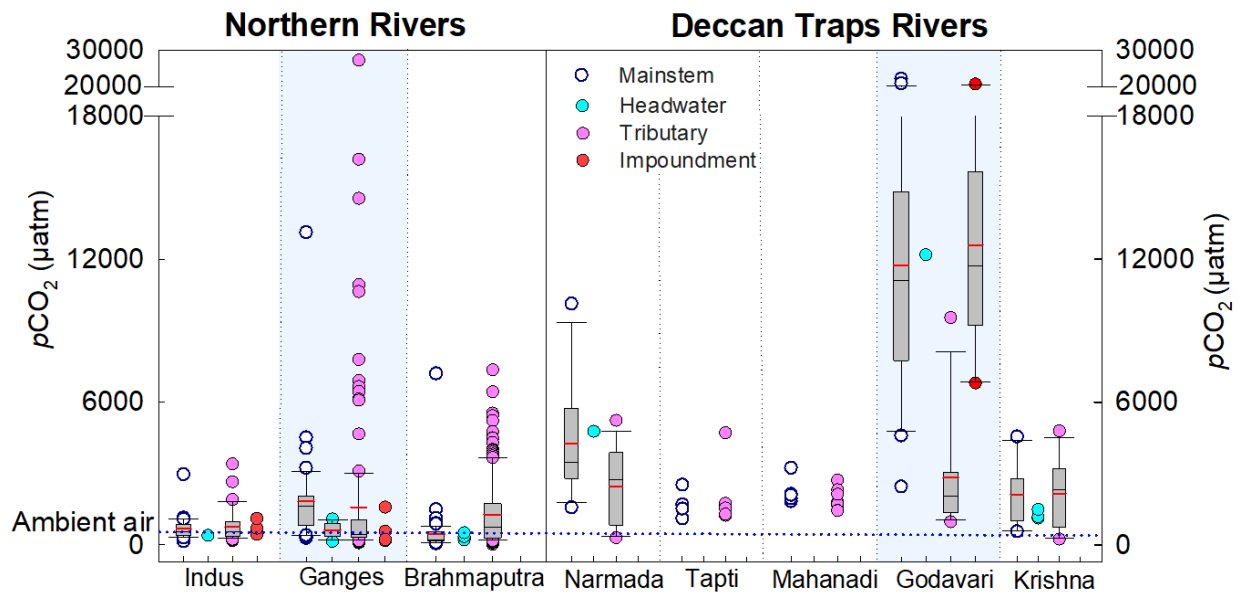


Fig. 2. Comparison of measured or estimated  $p\text{CO}_2$  among the mainstems, headwaters, tributaries, and impoundments across the Indian subcontinental river basins including the northern rivers (Ganges, Brahmaputra, and Indus) and rivers in the Deccan Traps (Narmada, Tapti, Mahanadi, Godavari, and Krishna). The tributary category of the Ganges basin includes wastewater drains and urban streams. The horizontal black and red lines of the box plots are the median and mean, respectively. Each box covers the 25th to 75th percentile, whereas the whiskers represent the 10th and 90th percentile. The blue dotted line represents the mean ambient air  $\text{CO}_2$  level (436  $\mu\text{atm}$ ) measured in the Ganges basin. Original data points are presented for the small datasets ( $n < 10$ ). Refer to Table 1 for data sources.

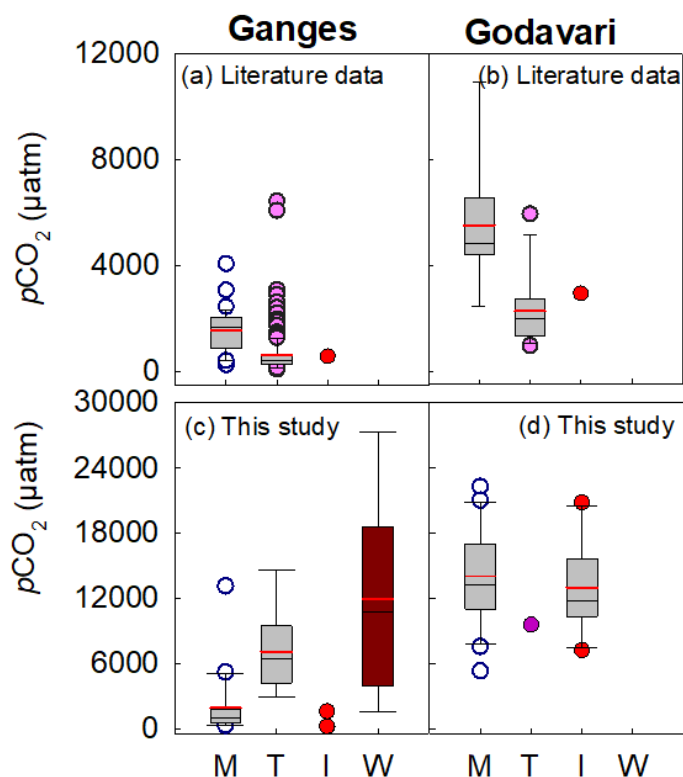


Fig. 3. Comparison of the literature data and field measurements of  $p\text{CO}_2$  among the mainstems (M), tributaries (T), impoundments (I), and wastewater drains or urban streams (W) across the Ganges and Godavari. While (a) and (b) show calculated literature data, (c) and (d) represent measured or calculated data from the field surveys of this study. The horizontal black and red lines of the box plots are the median and mean, respectively. The small data sets ( $n < 10$ ) are presented as original data points, not as box plots. Headwater streams were included in the mainstem or tributary category depending on location.

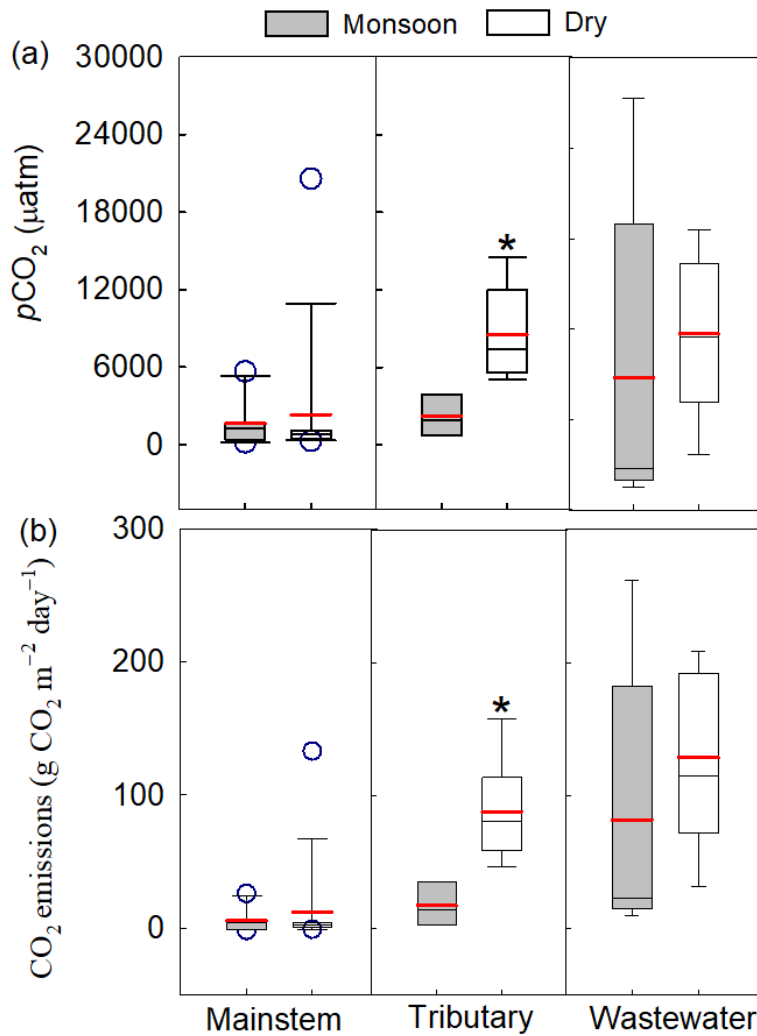


Fig. 4. Seasonal comparison of (a)  $p\text{CO}_2$  and (b)  $\text{CO}_2$  emissions per unit surface area in the mainstems, tributaries, and wastewater drains or urban streams of the Ganges basin between monsoon and dry seasons. Refer to Methods for the gas transfer velocity values ( $k_1$ ) used to estimate  $\text{CO}_2$  emissions. The horizontal black and red lines of the box plots are the median and mean, respectively. Asterisks indicate significant seasonal differences for each of the mainstems, tributaries, and wastewater drains or urban streams (t-test;  $p < 0.05$ ). Headwater streams and impounded sites were included in the mainstem category.

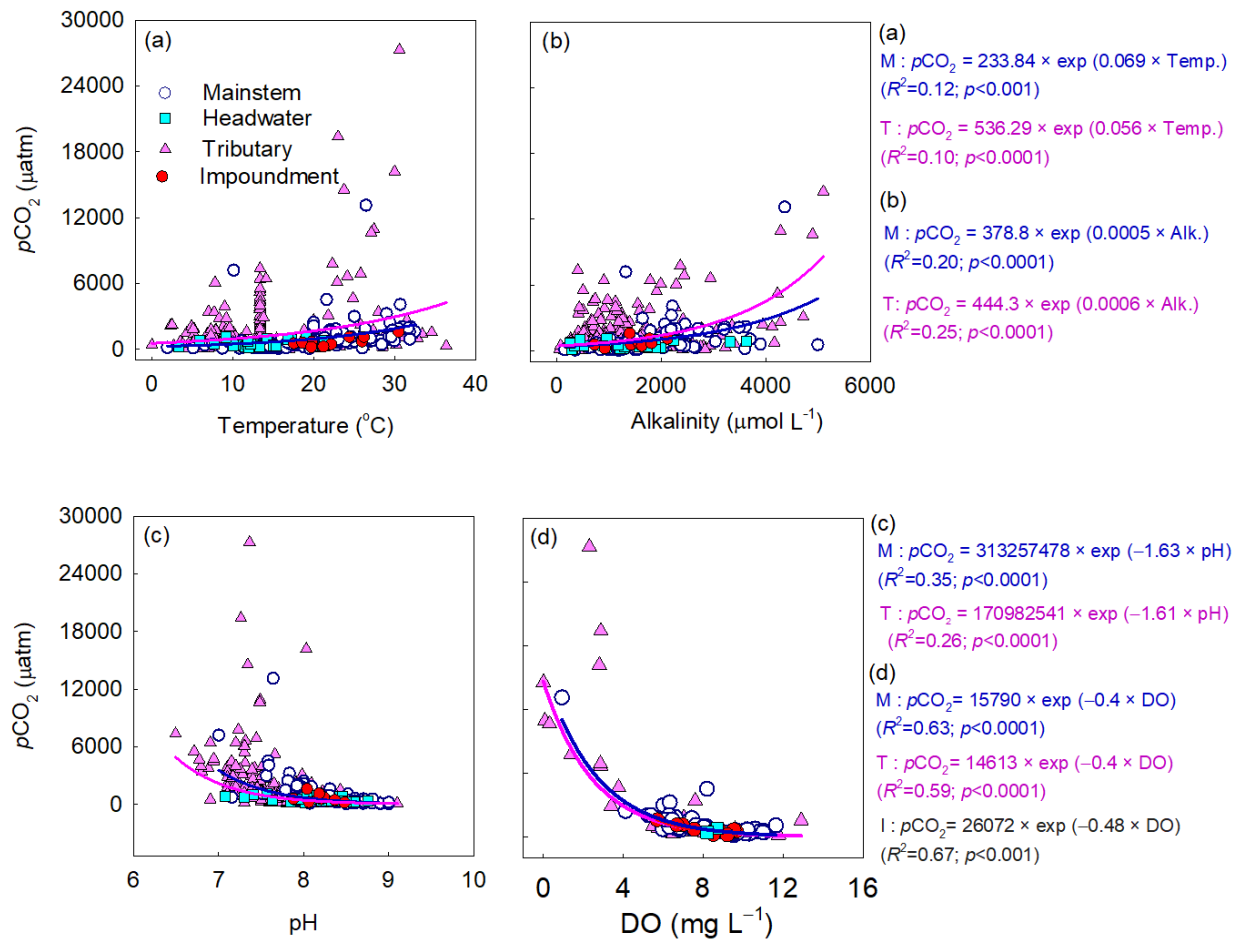


Fig. 5. Relationship between water quality parameters (a: temperature; b: alkalinity; c: pH; d: DO) and  $p\text{CO}_2$  for the mainstem reaches and tributaries of the northern rivers (Ganges, Brahmaputra, and Indus). The significant relationship ( $p<0.05$ ) for each of headwater streams (H), mainstems (M), tributaries (T), and impoundments (I) is indicated by the best-fit regression line.



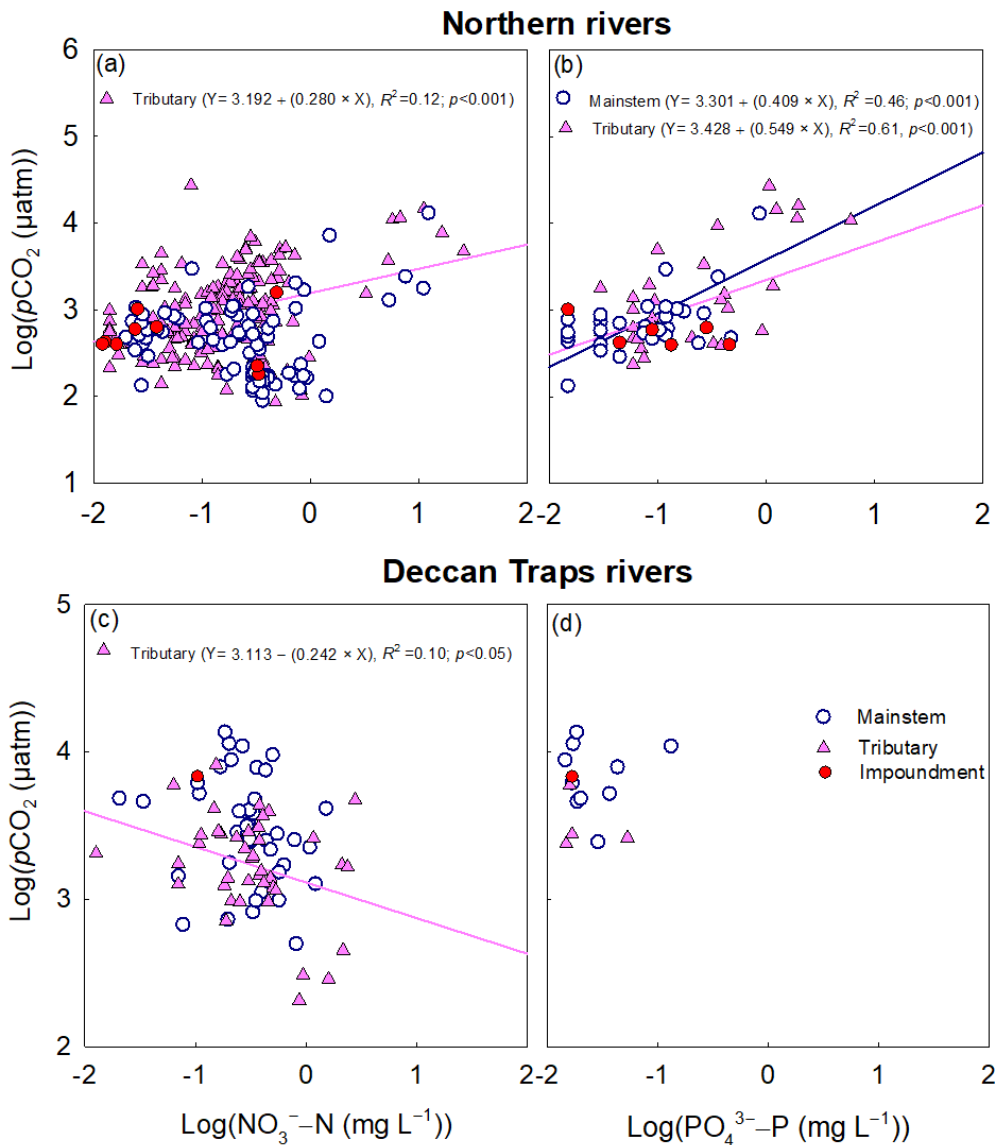


Fig. 6. Relationship between the log-transformed nutrient concentrations and  $p\text{CO}_2$  in the rivers of the Indian subcontinent. (a)  $\text{NO}_3^-$ -N concentrations in the mainstems ( $n=78$ ), tributaries ( $n=176$ ), and impoundments ( $n=9$ ) where DIN ( $\text{NO}_3^-$ -N +  $\text{NH}_4^+$ -N) concentrations in the Ganges River were used instead of  $\text{NO}_3^-$ -N concentrations; (b)  $\text{PO}_4^{3-}$ -P concentrations in the mainstems ( $n=29$ ), tributaries ( $n=33$ ), and impoundments ( $n=6$ ) across the northern rivers (Ganges, Brahmaputra, and Indus); (c)  $\text{NO}_3^-$ -N concentrations in the mainstems ( $n=40$ ) and tributaries ( $n=41$ ); (d)  $\text{PO}_4^{3-}$ -P concentrations in the mainstems ( $n=10$ ), tributaries ( $n=4$ ) in the Deccan Traps (data available only for the Godavari). Only significant relationship ( $p < 0.05$ ) is indicated by a regression line through the plot. Headwater streams were included in the mainstem or tributary category depending on location.

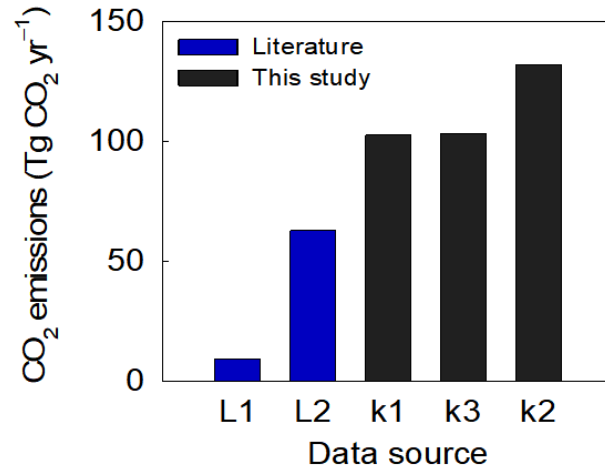


Fig. 7. Estimates of CO<sub>2</sub> emissions from the inland waters of the Indian subcontinent. The sources of literature data include Panneer Selvam et al. (2014) for L1 and Li & Bush (2015) for L2. Note that all estimates of CO<sub>2</sub> emissions are provided for the same surface area estimate of the subcontinental inland waters (44,282 km<sup>2</sup>). Refer to Methods for the three gas transfer velocity values (*k*1–*k*3) used to estimate CO<sub>2</sub> emissions in this study.

## Supporting Information for

### **Reassessing riverine carbon dioxide emissions from the Indian subcontinent**

Omme K. Nayna<sup>a</sup>, Vedula V.S.S. Sarma<sup>b</sup>, Most Shirina Begum<sup>a</sup>, Jens Hartmann<sup>c</sup>, Sanjeev Kumar<sup>d</sup>, Shafi M. Tareq<sup>e</sup>, Ji-Hyung Park<sup>a</sup>

<sup>a</sup>Department of Environmental Science and Engineering, Ewha Womans University, Seoul 03760, Republic of Korea

<sup>b</sup>National Institute of Oceanography, Council of Scientific and Industrial Research, Visakhapatnam, India

<sup>c</sup>Institute for Geology, University of Hamburg, Hamburg 20146, Germany

<sup>d</sup>Geosciences Division, Physical Research Laboratory, Ahmedabad 380009, India

<sup>e</sup>Department of Environmental Sciences, Jahangirnagar University, Dhaka 1342, Bangladesh

#### **Contents of this file**

Text S1 to S2

Tables S1 to S4

Figures S1 to S4

References

#### **Introduction**

This supporting information provides detailed descriptions of the study site including three northern rivers (Text S1) and four Deccan Traps rivers (Text S2) in the Indian subcontinent as along with Tables S1–S4, Figures S1–S4, and references.

### **Text S1: Northern rivers**

The northern rivers (Ganges, Brahmaputra, and Indus) originate in the Himalayas. The Ganges is a transboundary river that flows across the Trans-Gangetic plains in India to Bangladesh. The mainstem “Ganga” in India (the tributary called Bhagirathi) originates from the Gangotri glaciers and, after integrating major tributaries Yamuna, Gomti, Ghaghara, Gandaki, and Kosi, flows through Bangladesh as a distributary named the Padma. The Padma receives the Brahmaputra and Meghna and then empties into the Bay of Bengal through the lower Meghna estuary. The total length of the Ganges is 2,515 km (Parua, 2010), with a drainage area of  $1.05 \times 10^6 \text{ km}^2$  (Meybeck and Ragu, 2012) and an average annual discharge of  $490 \text{ km}^3 \cdot \text{yr}^{-1}$  (Milliman and Farnsworth, 2011). The Yamuna branch originates from the Yamunotri glaciers and merges with the Ganga branch at Allahabad. The Hooghly distributary flows through the West Bengal state of India from the Farakka Barrage near Murshidabad and meets the Bay of Bengal through the Hooghly estuary. The Brahmaputra originates in the Tibetan Plateau, flows through China and India, merges with the Ganges mainstem in Aricha, Bangladesh, and empties into the Bay of Bengal through the lower Meghna estuary. The average annual discharge of the Brahmaputra is  $630 \text{ km}^3 \cdot \text{yr}^{-1}$  (Milliman and Farnsworth, 2011), and  $1,270 \text{ km}^3 \cdot \text{yr}^{-1}$  for the lower reach of the Ganges-Brahmaputra system (downstream of the confluence with the Meghna; Milliman and Farnsworth, 2011). The Indus originates from the western Tibet and the Higher Himalayan region. After joining several left-bank tributaries (e.g, Zaskar and Sutlej) and right-bank tributaries (e.g., Shyok and Gumal), the Indus mainstem flows through Pakistan and empties into the Arabian Sea. The Indus traverses 3,000 km (Karim and Veizer, 2000) and has an average annual discharge of  $48 \text{ km}^3 \cdot \text{yr}^{-1}$  (Milliman and Farnsworth, 2011).

### **Text S2: Rivers originating from the Deccan Traps**

The Deccan volcanic province, referred to as the Deccan Traps, is located in central-western India (Fig.1). Four rivers originating from the Deccan Traps (Narmada, Tapti, Godavari, and Krishna) and the Mahanadi that flows through a rift connected to the Deccan Traps are here referred to as the Deccan Traps rivers. The Godavari is one of the largest monsoonal rivers in India and originates near Nasik in the Western Ghats, approximately 80 km inland from the western coast of India (Jha et al., 2009). It has a catchment area of  $3.1 \times 10^5 \text{ km}^2$  containing 25

tributaries (Gupta, 2001). The river traverses 1,480 km before draining into the Bay of Bengal, with an average annual discharge of  $70 \text{ km}^3 \cdot \text{yr}^{-1}$  (Prasad et al., 2013). The Godavari is dammed at 350 locations (Khedkar et al., 2014) to meet the demand for irrigation and domestic consumption, while Prasad et al. (2013) reported only five major dams. The river has four major tributaries: Manjara, Pranhita, Indravati, and Sabri (Jha et al., 2009). The Mahanadi originates near Nagari in the Indian state of Chhattisgarh, has a catchment area of  $140,000 \text{ km}^2$ , and discharges over  $50 \text{ km}^3 \cdot \text{yr}^{-1}$  into the Bay of Bengal (Milliman & Farnsworth, 2011; Panigrahy and Raymahashay, 2005). The Pairi, Seonath, Jonk, Hasdo, Mand, Ib, and Tel are all major tributaries (Panigrahy and Raymahashay, 2005). The Krishna has a total drainage area of  $260,000 \text{ km}^2$  (Milliman and Farnsworth, 2011), of which  $66,810 \text{ km}^2$  (26%) lies in the Deccan Traps (Das et al., 2005) and discharges  $37 \text{ km}^3 \cdot \text{yr}^{-1}$  into the Bay of Bengal (Milliman and Farnsworth, 2011). The Krishna merges with the Bhima at Nivrutti Sangamam. The Narmada is the largest west flowing river based on water discharge ( $38 \text{ km}^3 \cdot \text{yr}^{-1}$ ) and catchment area ( $98,796 \text{ km}^2$ ; Gupta et al., 2011). It originates as groundwater seepage (Narmada Kund) on the Amarkantak Plateau in the state of Madhya Pradesh. The Tapi originating from the Satpura range in the state of Madhya Pradesh (Dessert et al., 2001) has a catchment area of  $65,000 \text{ km}^2$  and annual discharge is  $9 \text{ km}^3 \cdot \text{yr}^{-1}$  (Milliman and Farnsworth, 2011). It converges with the Purna in northern Maharashtra and originates from the Satpura (Dessert et al., 2001).

River basin area and discharge data were obtained from Milliman and Farnsworth (2011). Pre-diversion discharge data are provided in parentheses for the rivers where discharge has substantially decreased in recent years because of river diversion, reservoir construction, and irrigation. Population data were taken from various sources including Park et al. (2018) and CIA World Factbook (<https://www.cia.gov/library/publications/the-world-factbook/index.html/>; last accessed on 10 January 2018). Asia total population is the population for all countries belonging to Asia and Oceania excluding Russia. South Asia total population for all countries belonging to South Asia (excluding Bhutan, Maldives, Afghanistan, and Iran) and Tibet. Listed rivers cover 90% discharge of Indian subcontinental rivers.

Table S1. Geographic and demographic features of the major river basins of the Indian subcontinent.

River		Receiving sea	Basin area (10 <sup>3</sup> km <sup>2</sup> )	Annual discharge (km <sup>3</sup> yr <sup>-1</sup> )	Population (×10 <sup>6</sup> )	Population density (km <sup>-2</sup> )	Annual discharge per capita (m <sup>3</sup> yr <sup>-1</sup> )
Northern rivers	Indus	Arabian Sea	980	5 (90)	220	224	23 (410)
	Ganges	Bay of Bengal	980	490	411	419	1193
	Brahmaputra	Bay of Bengal	670	630	209	312	3015
Deccan Traps rivers	Narmada	Arabian Sea	99	23 (38)	39	390	596 (984)
	Tapti	Arabian Sea	65	9	25	390	355
	Mahanadi	Bay of Bengal	140	47 (54)	55	390	861 (989)
	Godavari	Bay of Bengal	310	92 (120)	121	390	761 (993)
	Krishna	Bay of Bengal	260	12 (62)	101	390	118 (611)
South Asia			4213	1662 (1859)	1702	404	976 (1092)
Asia			32 518 (32 518)	11 000 (13 196)	4835	148	2275
World			105 000 (106 326)	36 000 (38 170)	7345	70	4901

Table S2. Summary of sampling sites in the eight major river basins of the Indian subcontinent.

River	Sampling time	Component	Country	Sampling points
Indus	1994–2007	Headwater	India	1
		Mainstem	Pakistan	24
		Tributary		39
		Impoundment		6
Ganges	1982–2019	Headwater	India	<sup>a</sup> 2, <sup>b</sup> 16
		Mainstem	India, Bangladesh	<sup>a</sup> 19, <sup>b</sup> 34
		Tributary	India, Bangladesh	<sup>a</sup> 6, <sup>b</sup> 143
		Wastewater	India, Bangladesh	<sup>a</sup> 8
		Impoundment	India	<sup>a</sup> 3, <sup>b</sup> 1
Brahmaputra	2007–2018	Headwater	Tibet	6
		Mainstem	Tibet, India, Bangladesh	55
		Tributary	Tibet, India, Bangladesh	165
Narmada	2001–2004	Headwater	India	1
		Mainstem		12
		Tributary		13
Tapti	2001	Mainstem	India	4
		Tributary		7
Mahanadi	2005	Mainstem	India	5
		Tributary		8
Godavari	2009–2012	Headwater	India	<sup>a</sup> 1
		Mainstem		<sup>a</sup> 20, <sup>b</sup> 9
		Tributary		<sup>a</sup> 1, <sup>b</sup> 12
		Impoundment		<sup>a</sup> 10, <sup>b</sup> 1
Krishna	2001–2002	Headwater	India	3
		Mainstem		10
		Tributary		15

The number of sampling points in the Ganges and Godavari with field measurements indicated by ‘a’ and literature data indicated by ‘b’.

Table S3. Summary of  $p\text{CO}_2$  estimated or measured in the eight major rivers of the Indian subcontinent. The studied rivers account for 90% of discharge from the Indian subcontinent (Milliman and Farnsworth, 2011).

Rivers	Mean (range) of $p\text{CO}_2$ ( $\mu\text{atm}$ )					Data source
	Mainstem	Headwater	Tributary	Impoundment	Basin	
Indus	684 (148–2970)	402 (373–430)	761 (172–3398)	757 (439–1117)	725 (148–3398)	Qu et al., 2017b, GLORICH <sup>a</sup>
Ganges	1855 (292–13 120)	625 (150–1087)	1575 <sup>b</sup> (88–27 290)	641 (180–1585)	1538 (88–27 290)	This study; Manaka et al., 2015; Samanta et al., 2015; Dutta et al., 2019; GLORICH <sup>a</sup>
Brahmaputra	468 (62–7198)	303 (209–513)	1284 (28–7348)		1059 (28–7348)	This study; Huang et al., 2011; Manaka et al., 2015; Qu et al., 2017a; Qu et al., 2017b; GLORICH <sup>a</sup> ,
Narmada	4260 (1580–10 129)	4768	2454 (304–5226)		3377 (304–10 129)	Dessert et al., 2001; Gupta et al., 2011
Tapti	1718 (1115–2528)		1982 (1238–4707)		1886 (1115–4707)	Dessert et al., 2001
Mahanadi	2253 (1833–3237)		1901 (1434–2727)		2036 (1434–3237)	Panigrahy and Raymahashay, 2005
Godavari	11 737 (2452–22 261)	12 177	2819 (969–9544)	12 595 (6798–20 796)	9599 (969–22 261)	This study; Dessert et al., 2001; Jha et al., 2009
Krishna	2116 (571–4549)	1264 (1125–1485)	2154 (238–4787)		2045 (238–4787)	GLORICH <sup>a</sup>
Total					2783 (28–27 290)	

<sup>a</sup>GLORICH: Global River Chemistry Database (Hartmann et al., 2014). <sup>b</sup>This category also includes wastewater drains or urban streams.



Table S4. Summary of the areal  $F_{CO_2}$  ( $\text{g CO}_2 \text{ m}^{-2} \text{ day}^{-1}$ ) from the eight major rivers of the Indian subcontinent. The  $F_{CO_2}$  is presented as the average per unit surface area, with the range calculated from three gas transfer velocity values ( $k_1$ – $k_3$ ).

Rivers	Mean (range) of $F_{CO_2}$ ( $\text{g CO}_2 \text{ m}^{-2} \text{ day}^{-1}$ )				
	Mainstem	Headwater	Tributary	Impoundment	Basin
Indus	1.7 (-2.5–20.2)	-0.8	4.1 (-4.8–47.4)	2.1 (0.02–5.2)	3.0 (-4.8–47.4)
Ganges	9.1 (-1.2–100.9)	2.5 (-4.7–10.7)	13.0 <sup>a</sup> (-6.3–355.7)	1.2 (-2.2–7.6)	11.2 (-6.3–355.7)
Brahmaputra	0.2 (-4.7–78.4)	-1.9 (-4.1–1.4)	13.9 (-9.3–166.6)		10.1 (-9.3–166.6)
Northern rivers	3.5 (-4.7–100.9)	1.1 (-4.7–10.7)	12.4 (-9.3–355.7)	1.7 (-2.2–7.6)	9.5 (-9.3–355.7)
Narmada	23.4 (6–63.8)	46.3	22.5 (-1.7–63.4)		23.8 (-1.7–63.8)
Tapti	7.8 (3.4–13.8)		17.3 (8.0–56.6)		13.9 (3.4–56.6)
Mahanadi	10.7 (7.0–17.6)		15.7 (6.3–29.0)		13.7 (6.3–29.0)
Godavari	67.7 (10.4–143.6)	120.8	25.5 (5.2–112.6)	85.4 (31.3–251.6)	61.4 (5.2–251.6)
Krishna	10.6 (0.7–27.7)	9.5 (7.1–14.2)	19.3 (-2.6–59.0)		15.1 (-2.6–59.0)
Deccan Traps rivers	39.2 (0.7–143.6)	39.1 (7.1–159.2)	20.7 (-2.6–112.6)	85.4 (31.3–251.6)	34.7 (-2.6–251.6)
Total					19.0 (-9.3–355.7)

<sup>a</sup>This also includes wastewater drains or urban streams.

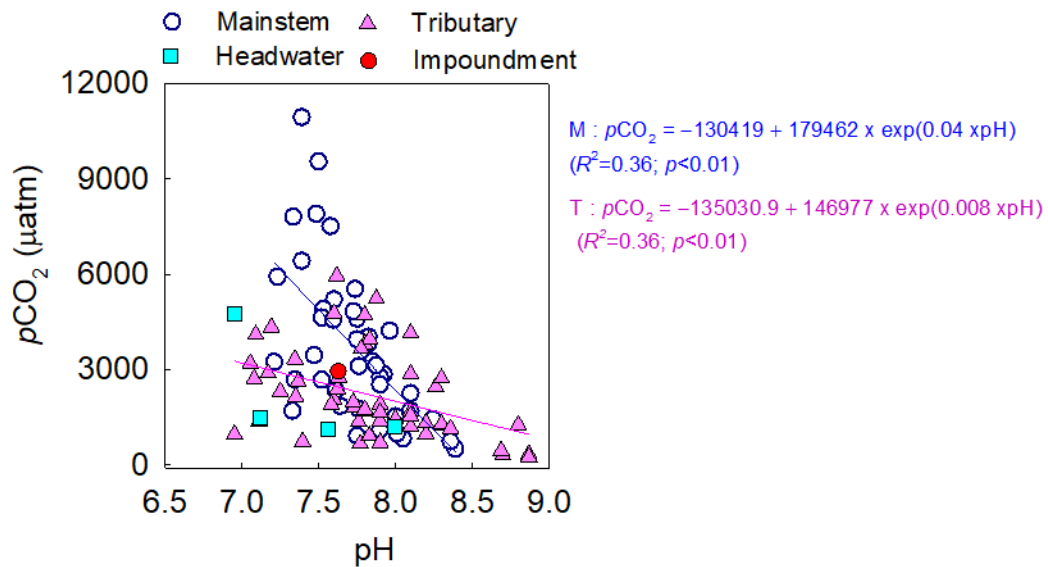


Fig. S1. Relationships between pH and  $pCO_2$  in the mainstems and tributaries of the rivers in the Deccan Traps (Narmada, Tapi, Mahanadi, Godavari, and Krishna). The significant relationship ( $p<0.01$ ) for each of the headwater streams (H), mainstems (M), tributaries (T), and impoundments (I) is indicated by the best-fit regression line.

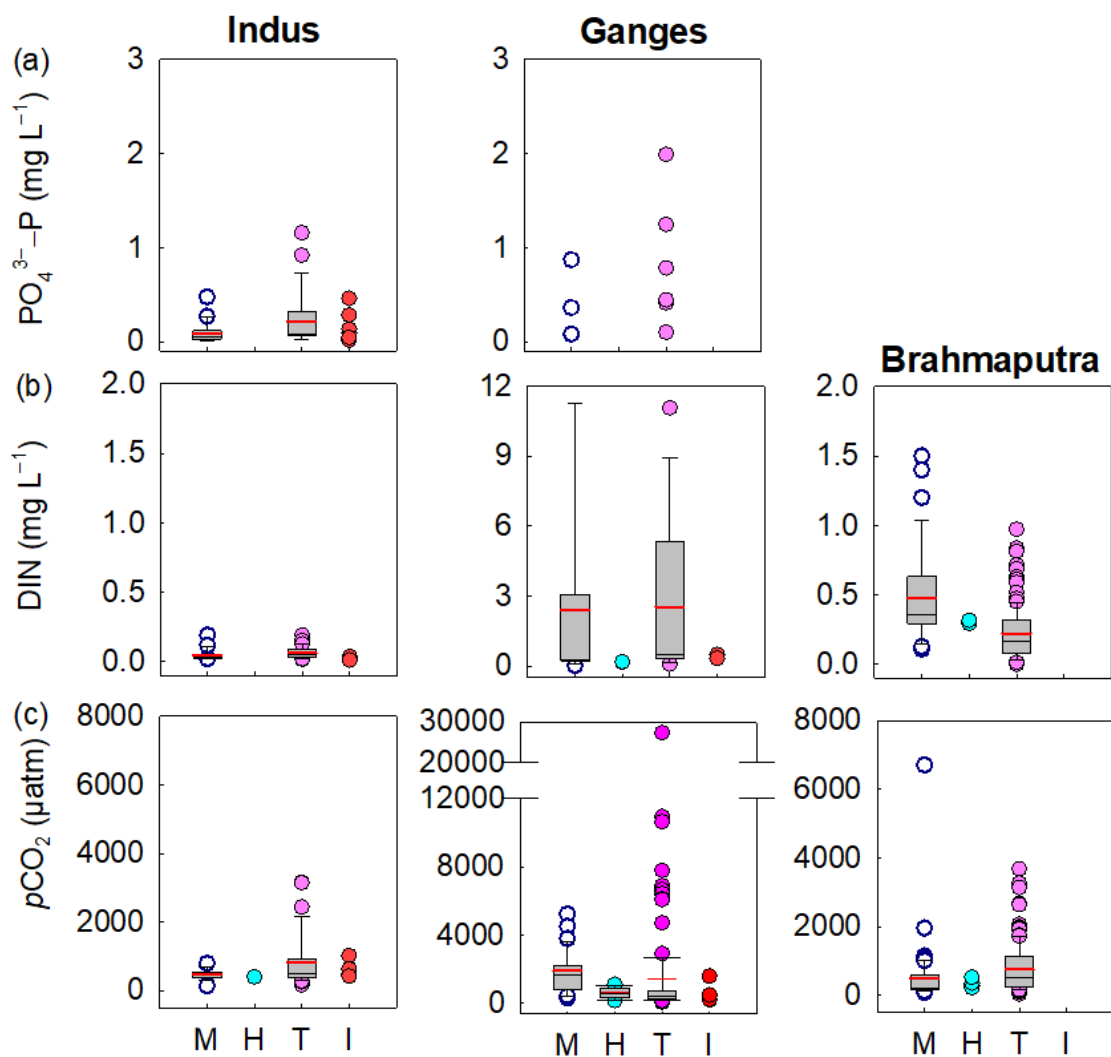


Fig. S2A. (a) Box plots showing spatial variations in riverine  $pCO_2$ ,  $NO_3^- - N$ , and  $PO_4^{3-} - P$  in the mainstems (M), headwaters (H), tributaries (T), and impoundments (I) across the northern rivers of the Indian subcontinent (Ganges, Brahmaputra, and Indus). The horizontal black and red lines of the box plots are the median and mean, respectively. Note that DIN (DIN:  $NO_3^- - N + NH_4^+ - N$ ) and  $NO_3^- - N$  data are presented for the Ganges and the other rivers, respectively (b), where other two rivers present only  $NO_3^- - N$  data. The small-number ( $n < 10$ ) data are presented as original data points, not as box plot.

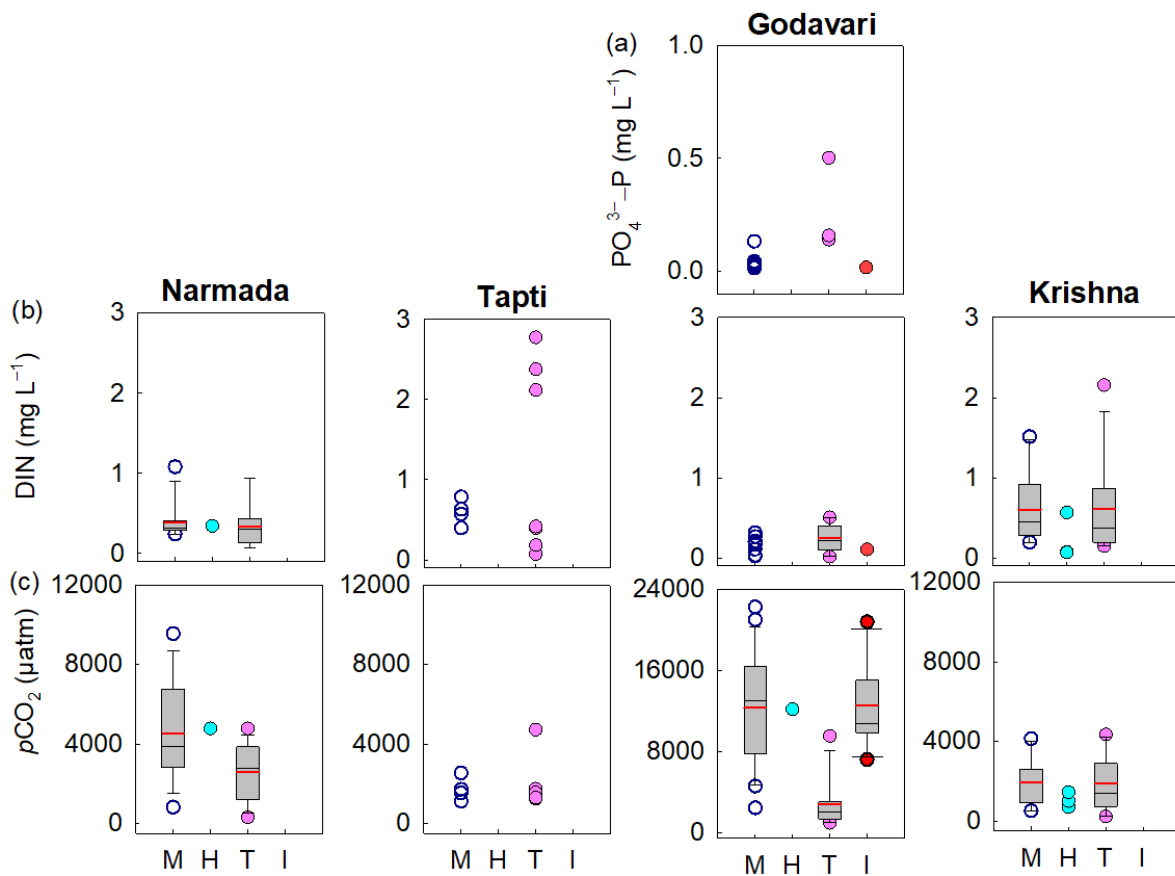


Fig. S2B. (b) Box plots showing spatial variations in riverine  $pCO_2$ ,  $NO_3^- - N$ , and  $PO_4^{3-} - P$  in the mainstems (M), headwaters (H), tributaries (T), and impoundments (I) across the Deccan Traps rivers of the Indian subcontinent (Narmada, Tapti, Godavari, and Krishna). Note that DIN (DIN:  $NO_3^- - N + NH_4^+ - N$ ) and  $NO_3^- - N$  data are presented for the Deccan Traps rivers (b), where the Krishna River presents only  $NO_3^- - N$  data. The horizontal black and red lines of the box plots indicate the median and mean value, respectively. The small-number ( $n < 10$ ) data are presented as original data points, not as box plot.

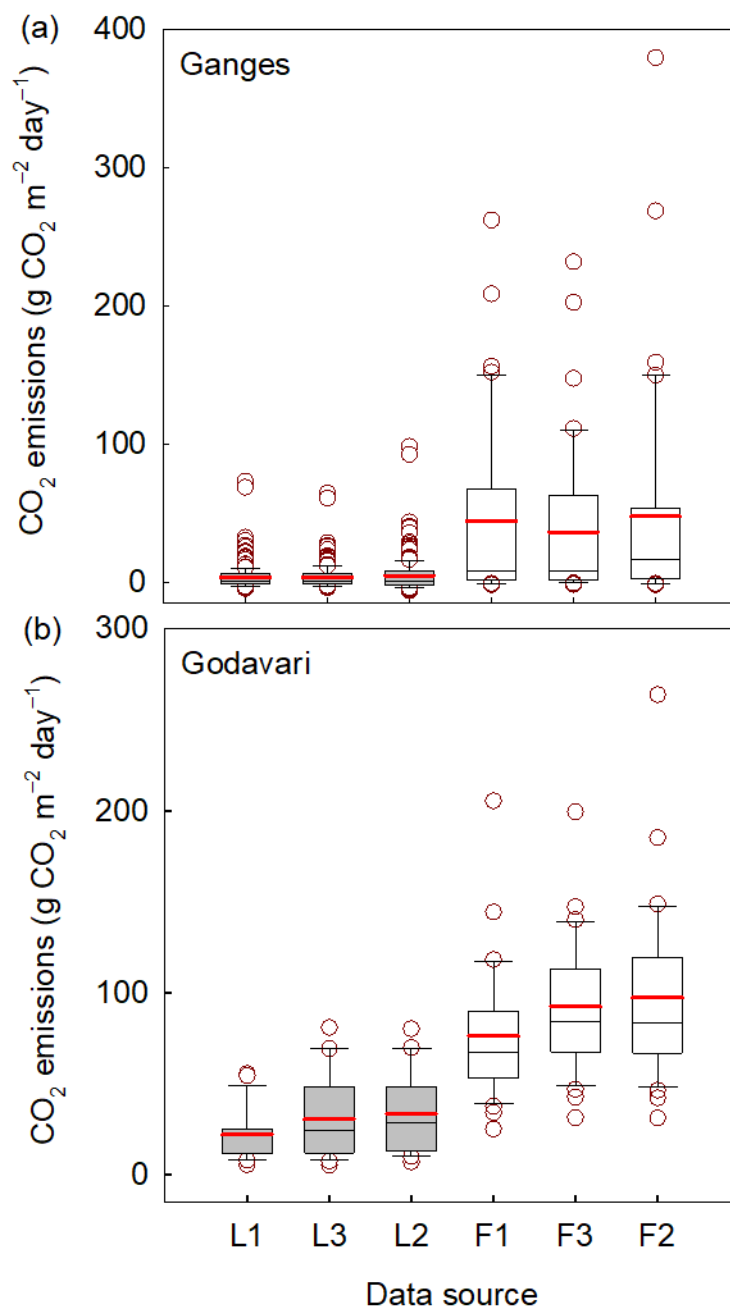


Fig. S3. Estimates of CO<sub>2</sub> emissions per unit surface area from the Ganges (a) and Godavari (b). Three gas transfer velocity values ( $k_1$ – $k_3$ ; refer to Methods) were used to estimate CO<sub>2</sub> emissions with literature data (L1–L3) and new field data obtained in this study (F1–F3). The horizontal black and red lines of the box plots represent the median and mean value, respectively.

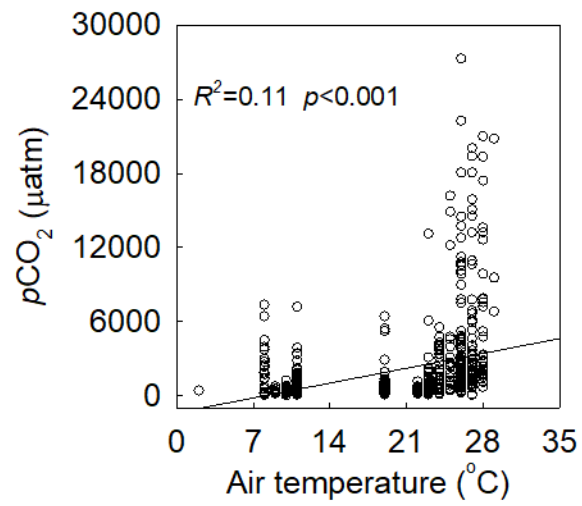


Fig. S4. Relationships between air temperature and  $p\text{CO}_2$  along the eight major rivers of the Indian subcontinent. The significant relationship ( $p < 0.001$ ) is indicated by a solid regression line through the plot.

## References

- Das, A., Krishnaswami, S., Sarin, M. M., Pande, K., 2005. Chemical weathering in the Krishna basin and Western Ghats of the Deccan Traps, India: rates of basalt weathering and their controls. *Geochim. Cosmochim. Acta* 69, 2067–2084. <https://doi.org/10.1016/j.gca.2004.10.014>
- Dessert, C., Dupre, B., Francois, L. M., Schott, J., Gaillardet, J., Chakrapani, G., Bajpai, S., 2001. Erosion of Deccan Traps determined by river geochemistry: impact on the global climate and the  $^{87}\text{Sr}/^{86}\text{Sr}$  ratio of seawater. *Earth Planet. Sci. Lett.* 188, 459–474. [https://doi.org/10.1016/S0012-821X\(01\)00317-X](https://doi.org/10.1016/S0012-821X(01)00317-X)
- Dutta, M. K., Kumar, S., Mukherjee, R., Sanyal, P., Mukhopadhyay, S. K., 2019. The post-monsoon carbon biogeochemistry of the Hooghly-Sundarbans estuarine system under different levels of anthropogenic impacts. *Biogeosciences*, 16, 289–307. <https://doi.org/10.5194/bg-16-289-2019>
- Gupta, L.P., 2001. Nature of sedimentary organic matter in the lower reaches of the Godavari River Basin, India. *J. Asian Earth Sci.* 19, 727–736. [https://doi.org/10.1016/S1367-9120\(01\)00003-7](https://doi.org/10.1016/S1367-9120(01)00003-7)
- Gupta, H., Chakrapani, G. J., Selvaraj, K., Kao, S. J., 2011. The fluvial geochemistry, contributions of silicate, carbonate, and saline–alkaline components to chemical weathering flux and controlling parameters: Narmada River (Deccan Traps), India. *Geochim. Cosmochim. Acta* 75, 800–824. <https://doi.org/10.1016/j.gca.2010.11.010>
- Hartmann, J., Lauerwald, R., Moosdorf, N., 2014. A brief overview of the GLOBAL River Chemistry Database, GLORICH. *Procedia Earth. Planet. Sci.* 10, 23–27. <https://doi.org/10.1016/j.proeps.2014.08.005>
- Huang, X., Sillanpaa, M., Gjessing, E. T., Peraniemi, S., Vogt, R. D., 2011. Water quality in the southern Tibetan Plateau: chemical evaluation of the Yarlung Tsangpo (Brahmaputra). *River Res. Applic.* 27, 113–121. <https://doi.org/10.1002/rra.1332>
- Jha, P. K., Tiwari, J., Singh, U. K., Kumar, M., Subramanian, V., 2009. Chemical weathering and associated  $\text{CO}_2$  consumption in the Godavari River basin, India. *Chem. Geol.* 264, 364–374. <https://doi.org/10.1016/j.chemgeo.2009.03.025>
- Karim, A., Veizer, J., 2000. Weathering processes in the Indus river basin: implications from riverine carbon, sulfur, oxygen and strontium isotopes. *Chem. Geol.* 170, 153–177. [https://doi.org/10.1016/S0009-2541\(99\)00246-6](https://doi.org/10.1016/S0009-2541(99)00246-6)
- Khedkar, G. D., Lutzky, S., Rathod, S., Kalyankar, A., David, L., 2014. A dual role of dams in fragmentation and support of fish diversity across the Godavari River basin in India. *Ecohydrology* 7, <https://doi.org/10.1002/eco.1470>
- Manaka, T., Ushie, H., Araoka, D., Otani, S., Inamura, A., Suzuki, A., Zakir Hossain, H. M., Kawahata, H., 2015. Spatial and seasonal variation in surface water  $p\text{CO}_2$  in the Ganges,

- Brahmaputra, and Meghna Rivers on the Indian Subcontinent. *Aquat. Geochem.* 21, 437–458. <https://doi.org/10.1007/s10498-015-9262-2>
- Meybeck, M., Ragu, A., 2012. GEMS-GLORI world river discharge database. <https://doi.org/10.1594/PANGAEA.804574>
- Milliman, J. D., Farnsworth, K. L., 2011. River discharge to the coastal ocean: a global synthesis. Cambridge University Press, Cambridge, UK, 13–69.
- Panigrahy, B. K., Raymahashay, B. C., 2005. River water quality in weathered limestone: case study in upper Mahanadi basin, India. *J. Earth Syst. Sci.* 114, 533–543.
- Park, J.-H., Nayna, O. K., Begum, M. S., Chea, E., Hartmann, J., Keil, R. G., Kumar, S., Lu, X., Ran, L., Richey, J.E., Sarma, V.V.S.S., Tareq, S.M., Thi Xuan, D., Yu, R., 2018. Reviews and syntheses: anthropogenic perturbations to carbon fluxes in Asian river systems – concepts, emerging trends, and research challenges. *Biogeosciences* 15, 3049–3069. <https://doi.org/10.5194/bg-2017-549>
- Parua, P. K., 2010. The Ganga: Water use in the Indian subcontinent. Water Science and Technology Library: Springer Sciences, New York, USA, 64, 9.
- Prasad, M. H. K., Sarma, V. V. S. S., Krishna, M. S., Reddy, N. P. C., 2013. Carbon dioxide emissions from the tropical Dowleiswaram reservoir on the Godavari River, Southeast of India. *J. Water Resour. Prot.* 5, 534–545. <https://doi.org/10.4236/jwarp>
- Qu, B., Zhang, Y., Kang, S., Sillanpää, M., 2017a. Water chemistry of the southern Tibetan Plateau: an assessment of the Yarlung Tsangpo River basin. *Environ. Earth Sci.* 76, <https://doi.org/10.1007/s12665-017-6393-3>
- Qu, B., Aho, K. S., Li C., Kang, S., Sillanpää, M., Yan, F., Raymond, P. A., 2017b. Greenhouse gases emissions in rivers of the Tibetan Plateau. *Sci. Rep.* 7, <https://doi.org/10.1038/s41598-017-16552-6>
- Samanta, S., Dalai, T. K., Pattanaik, J. K., Rai, S. K., Mazumdar, A., 2015. Dissolved inorganic carbon (DIC) and its  $\delta^{13}\text{C}$  in the Ganga (Hooghly) River estuary, India: evidence of DIC generation via organic carbon degradation and carbonate dissolution. *Geochim. Cosmochim. Acta* 165, 226–248. <https://doi.org/10.1016/j.gca.2015.05.040>